Numerical Simulations of the Impact of Large Wind Farms on Local Climate

by

Yogesh Rao Kadiyala

A Thesis Presented in Partial Fulfillment
of the Requirements for the Degree
Master of Science

Approved April 2015 by the
Graduate Supervisory Committee:

Huei-Ping Huang, Chair
Jagannathan Rajagopalan
Ronald Calhoun

ARIZONA STATE UNIVERSITY

May 2015

ABSTRACT

Due to decrease in fossil fuel levels, the world is shifting focus towards renewable sources of energy. With an annual average growth rate of 25%, wind is one of the foremost source of harnessing cleaner energy for production of electricity. Wind turbines have been developed to tap power from wind. As a single wind turbine is insufficient, multiple turbines are installed forming a wind farm. Generally, wind farms can have hundreds to thousands of turbines concentrated in a small region. There have been multiple studies centering the influence of weather on such wind farms, but no substantial research focused on how wind farms effect local climate. Technological advances have allowed development of commercial wind turbines with a power output greater than 7.58 MW. This has led to a reduction in required number of turbines and has optimized land usage. Hence, current research considers higher power density compared to previous works that relied on wind farm density of 2 to 4 W/m^2. Simulations were performed using Weather Research and Forecasting software provided by NCAR. The region of simulation is Southern Oregon, with domains including both onshore and offshore wind farms. Unlike most previous works, where wind farms were considered to be on a flat ground, effects of topography have also been considered here. Study of seasonal effects over wind farms has provided better insight into changes in local wind direction. Analysis of mean velocity difference across wind farms at a height of 10m and 150m gives an understanding of wind velocity profiles. Results presented in this research tends to contradict earlier belief that velocity reduces throughout the farm. Large scale simulations have shown that sometimes, more than 50% of the farm can have an increased wind velocity of up to 1m/s at an altitude of 10m.

ACKNOWLEDGMENTS

I would like to thank Dr. Huei-Ping Huang for advising me and supporting me throughout my thesis. He has guided me through each and every step of this project. I would also like to thank Dr. Ronald Calhoun and Dr. Jagannathan Rajagopalan for presiding over my thesis committee.

I am also grateful to fellow graduate student, Samy Kamal for helping me setup WRF. His expertise in weather forecasting and post processing was invaluable.

I would like to acknowledge my friends, Sai Krishna Mantravadi and Sree Harsha Maddineni, for their valuable insights into this research.

TABLE OF CONTENTS

Page

APPENDIX Page

LIST OF TABLES

LIST OF FIGURES

Figure Page

Figure Page

Figure Page

Figure Page

CHAPTER 1

INTRODUCTION

Overview

As the world energy needs are increasing with declining resources of our fossil deposits, there is an increase in dependency on renewable energy. Energy needs to be harnessed by tapping areas which can provide maximum power production. One of the fastest growing renewable energy source is wind power. Due to increase in political, social and economic concern, wind power has been given a tremendous boost. The capacity of wind farms installed has increased from 24.3 GW in 2001 to 196.6 GW in 2010 (WWEA staff 2010). With an annual growth rate of 25%, wind energy is being harnessed competitively for large load demands as well. Since each wind turbine has a low rated capacity which is not adequate enough, multiple turbines are added leading to a wind farm. (Shen Lu 2014)

Figure 1.1 shows annual average wind speed over the United States. Southern part of Oregon and the northern part of California have been rated excellent ('Superb') in terms of resource potential, highest in wind power class, with power density at 800-1600 W/m^2 at a height of 50m and an average wind speed of 8.8-11.1 m/s (19.7-24.8 mph). Even though the average wind speed over land is approximated to 4.5-5 m/s, we will be neglecting it as our defined domain would be of the coast of Oregon. Hence, a little variation in wind speed would be observed as there is no major change in topography.

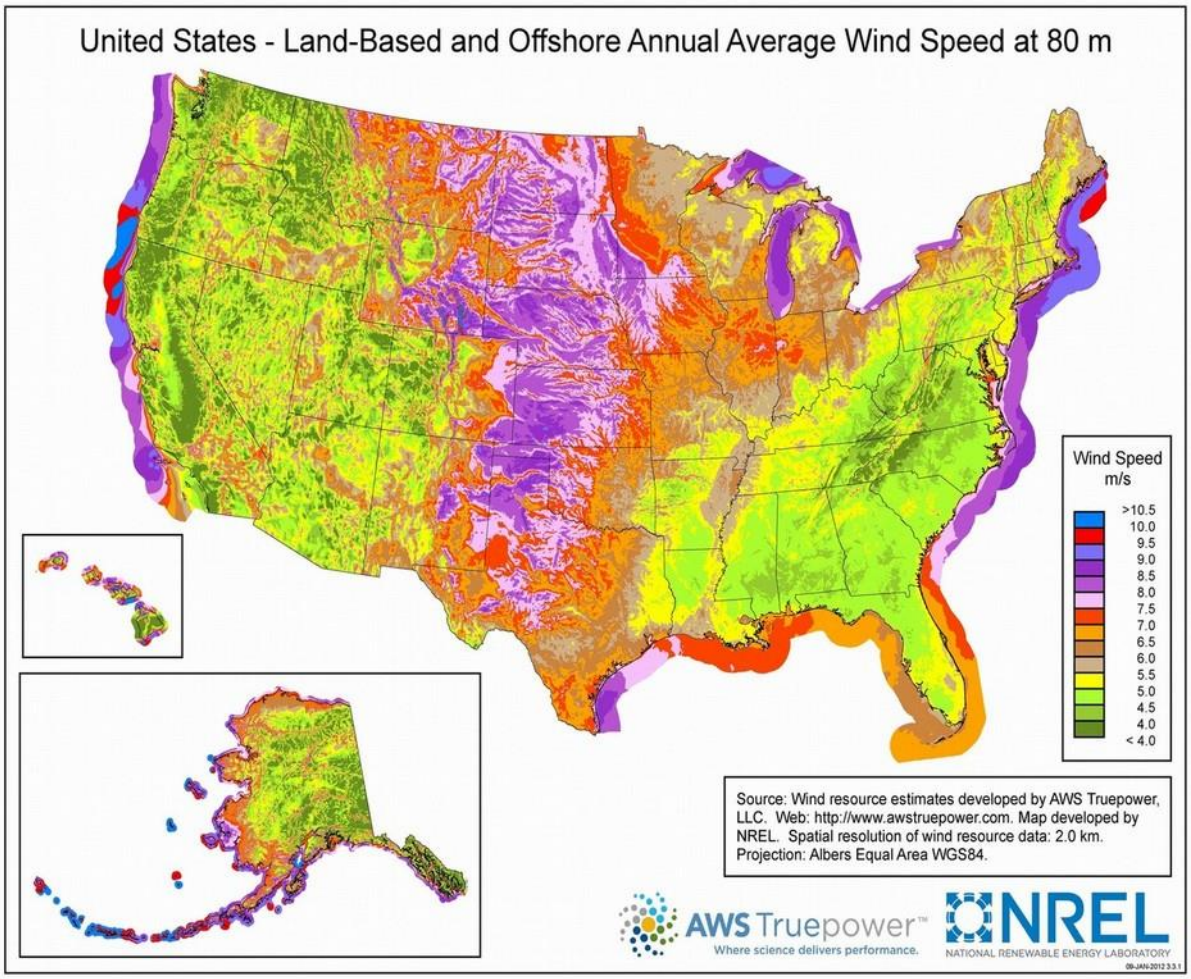

Figure 1.1. Represents onshore and offshore annual average wind speed at 80m (courtesy NREL)

Figure 1.2 shows that transmission lines of 1000KV voltage are not far from our planned wind farm simulations. This suggests, integration of wind farm to the power grid would not be very expensive since the cost of integration would be borne by wind farm developers. As initial setup costs are expensive, such features would reduce the financial burden.

With such estimates, capacity factor of wind farm can be aimed towards the higher end of the range (20% to 70%). This would help maintain or further reduce commercial wind energy price of 4 to 5 cents per kWh (Shaahid 2014).

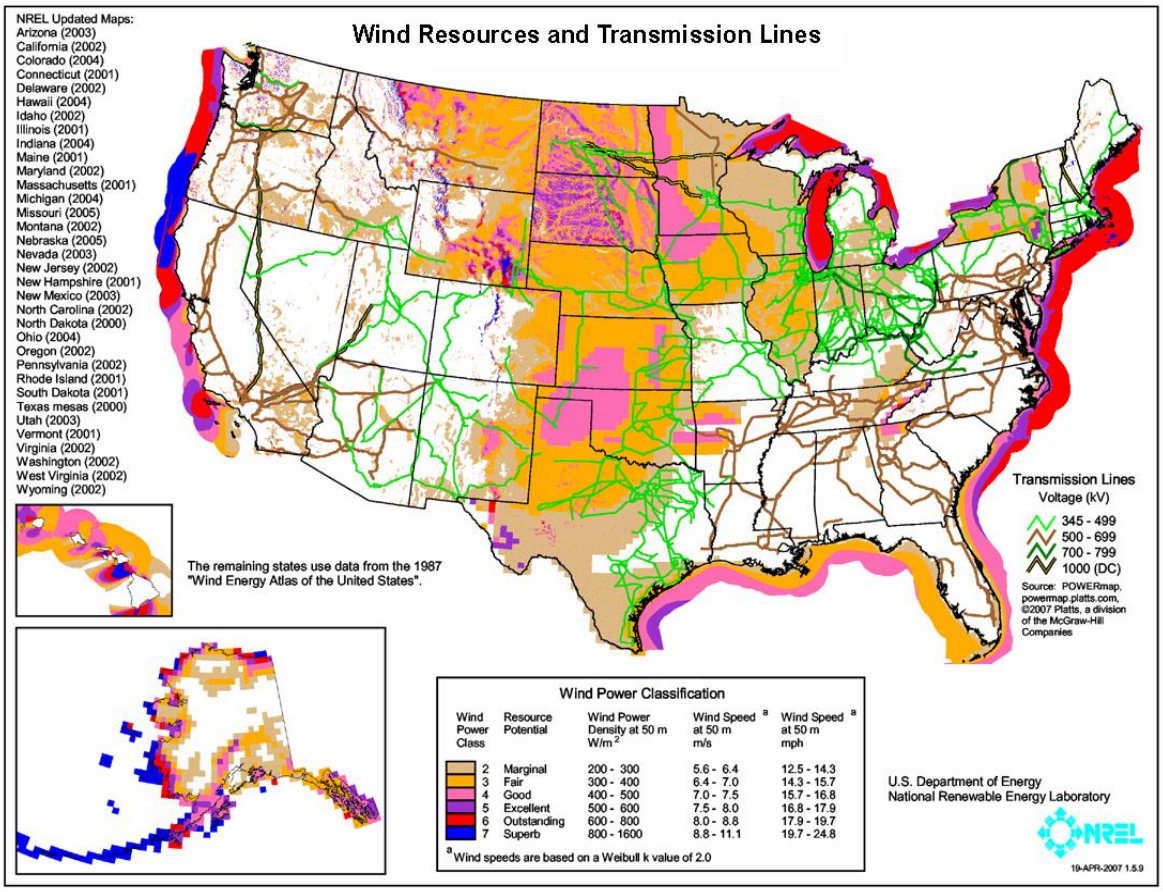

Figure 1.2. Representation of offshore wind resource and transmission lines across United States (Courtesy NREL)

Past Research

Until recent times, research has been conducted as to how well-defined an onshore Wind Farm (Roy 2010) or an offshore wind farm (Giannakopoulou 2014) effects local climate on a mesoscale. Even the effects of coastal wind farms conducted (Kim 2015) in Korea had nine Wind Turbines placed over the island, where the total capacity was 22 MW, with average wind speeds of 5-6 m/s.

The research conducted by Gopalan (2014) largely focuses on use of multiple tools such as Uwaske, Flowyo and HELIOS for wind turbine analysis with laminar and

turbulent inflows, including changes in spacing between wind turbines. Mehta (2014) discussed aerodynamics of wind farm, minimal effects of near and far wake on the result, and methods to address the far wake issues.

The offshore wind farm simulations performed by McCombs (2014) with 130 turbines on Lake Ontario calculated its impact on surface water and wave formation. Using Blade element momentum theory, Son (2014) concluded that changes in turbine spacing can result in changes of thrust and power coefficients.

Moorthys' (2014) analysis featured use of genetic algorithm to model optimal layout that can be modified according to changing turbine quantities, resulting in reduced wake and increased power generation.

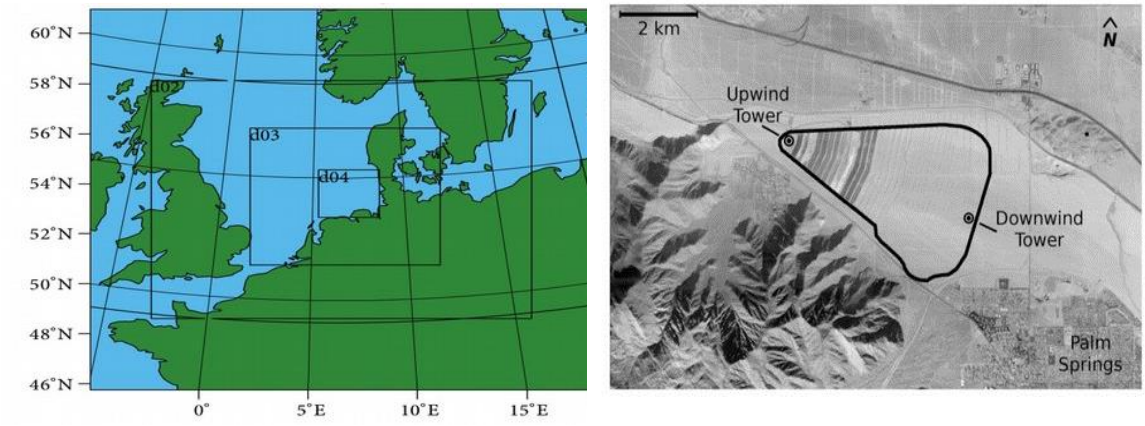

(a) (b)

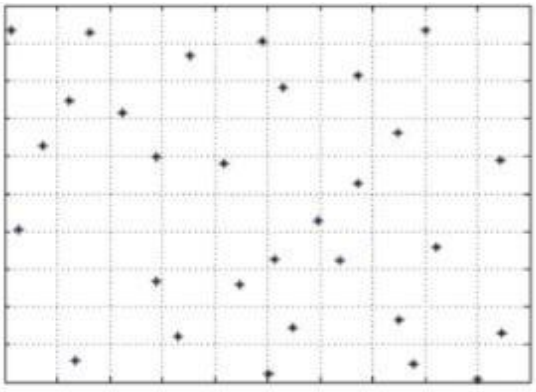

(c)

Figure 1.3. (a) Offshore domain, (b) Onshore domain, both represent and isolated wind farm area, (c) Layout of 30 wind turbines

Potential Contribution

There has not been much research conducted on sizable wind farms and their effects on local climate. This research would potentially bring to light, the impact of seasonal effects on atmosphere. As weather patterns do not change drastically over a period of time, it is beneficial to set up high speed wind farms. Since wind farm design used in this study has incorporated next generation wind turbines, whose power is twice that of turbines researched until now, it would provide gainful insights into effects of climate change.

This study tries to quantify weather changes in comparison with day and night, and effects of changing wind patterns on Wind energy. As winter weather has different temperature ranges compared to summer, seasonal effect over wind farms was considered in this study. Meteorological dates in January and July, considered as peaks in their respective seasonal months (as per National Center for Atmospheric Research), were used in this study.

This research utilized only square wind farm patterns, and not the ones provided by genetic algorithm or any of the variations provided by either Mosettis' or Marmidis' optimal layout. The focus of this work is study of wind velocity and mean wind velocity difference at altitudes of 10m and 150m.

Turbine spacing has been kept constant throughout the wind farm without any unallocated blocks in between. Changes in thrust and power coefficients is beyond the scope of this research. Since turbine configurations have been taken from a proven technology, study of blade aerodynamics is redundant.

CHAPTER 2

WEATHER RESEARCH AND FORECASTING MODEL

Overview of WRF

The model used here is called Weather Research and Forecasting (WRF), a mesoscale numerical weather prediction system used for atmospheric research and operational forecasting. The Advanced Research WRF (ARW) is a dynamic solver. The WRF systems' principal components are illustrated in figure 2.1. The WRF Software Framework (WSF) has dynamic solvers and physics packages, interacting with solvers like WRF-Var and WRF-Chem. There are two types of dynamic solvers in WSF: Advanced Research WRF (ARW) and Nonhydrostatic Mesoscale Model (NMM). ARW has been used in present research.

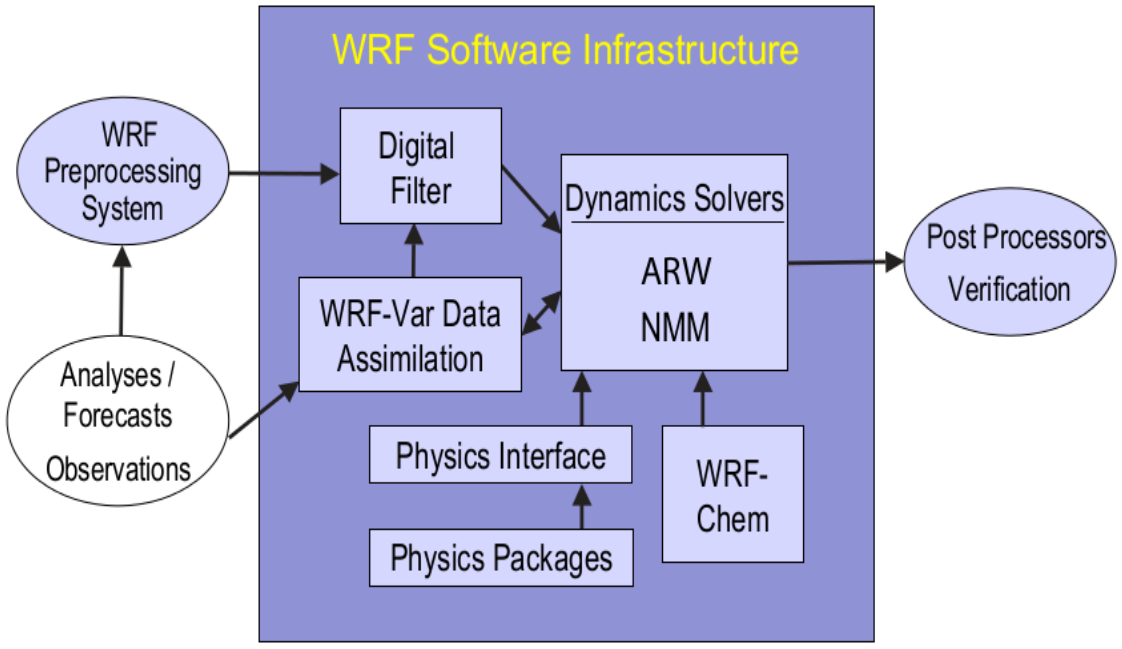

Figure 2.1. WRF system components (courtesy Skamarock 2008)

The WRF development was a collaborated effort between National Center for Atmospheric Research (NCAR), Air Force Weather Agency (AFWA), National Oceanic and Atmospheric Administration (NOAA), Naval Research Laboratory, National Centers for Environment Prediction (NCEP), Forecast Systems Laboratory (FSL), Federal Aviation Administration (FAA), and other participating universities.

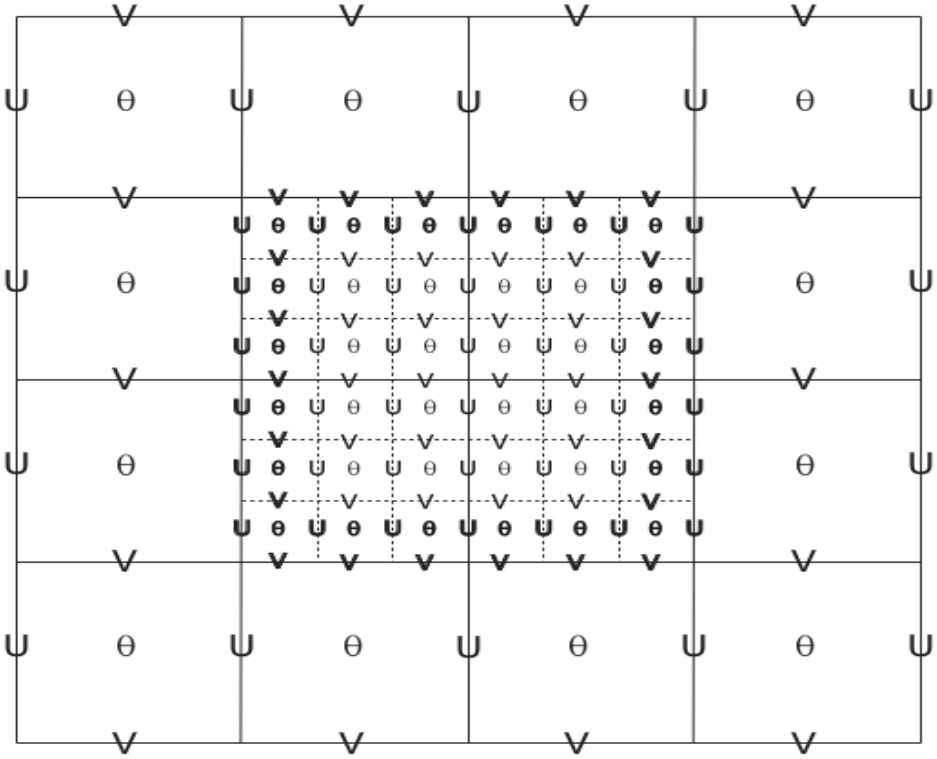

Figure 2.2. Arakawa-C grid staggering (courtesy Skamarock 2008)

WRF uses Arakawa-C grid staggering for variables shown in figure 2.2. This grid is the mass core of WRF which permits horizontal staggering and vertical stretching, which uses terrain-following hydrostatic pressure coordinate system. It utilizes complete Coriolis, 5^{th} order upwind advection scheme, 3^{rd} order Runge-Kutta split explicit time integration scheme, curvature and mapping terms (Salvação 2014).

The ARW, dynamic solver of WRF, has been used for executing simulations. It utilizes physics schemes, dynamics and numeric options, initialization routines, and data assimilation package (WRF-Var).

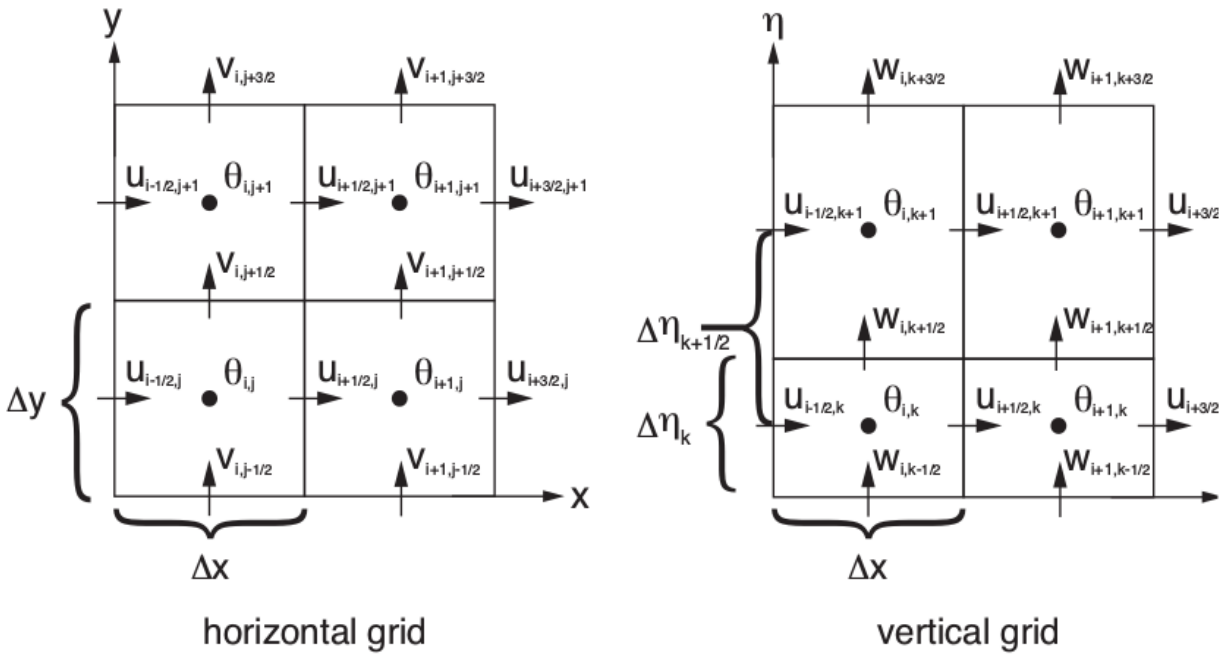

Figure 2.3. Horizontal and vertical grids of the ARW (courtesy Skamarock 2008)

In figure 2.3, normal velocities are staggered on half of grid length from grid points. Indices i, j and k indicate variables with location (x, y, η) = (iΔx, jΔy, kΔη). Location of θ denotes mass points. Similarly u, v and w are velocities in x, y and z direction. Column mass μ, which is not shown here is defined at mass points (i, j) on the discrete grid. Moisture variable q_m is defined at mass points and goepotential (denoted by φ) is defined at w points.

Mass points are also used to compute inverse density α and pressure p. Grid lengths Δx and Δy do not change in the model formation and remain constant throughout, whereas η is a terrain-following hydrostatic-pressure vertical coordinate. η =1 at surface

and η = 0 at top of the model. It decreases monotonically in the space between surface and the top. Where η is defined as:

$$\eta = \frac{(p_h - p_{ht})}{\mu}$$

$$\mu = p_{hs} - p_{ht}$$

Where, p_h = Hydrostatic component of pressure

p_{ht} = Top surface boundary

p_{hs} = Bottom surface boundary

μ(x,y) = mass per unit area

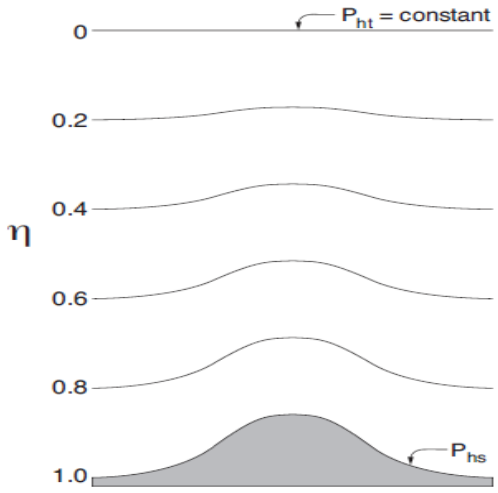

Figure 2.4. ARW η coordinate

The vertical sub-grid fluxes that are caused because of eddy transports within entire atmospheric column and not just the boundary layer, is the responsibility of planetary boundary layer (PBL). Explicit vertical diffusion is de-activated as PBL is activated and this handles the process. Surface layer and land-surface profiles provide the surface fluxes. PBL schemes are very useful as they provide flux profiles inside well-

mixed boundary layer and also the stable layer. Hence, it provides horizontal momentum and thermal atmospheric tendencies in the vertical direction of atmosphere. PBL schemes include stable saturation effects in vertical direction and also take dry mixing into account. The assumption that there exists a separation between resolved eddies and sub-grid eddies are one dimensional, holds true until the grid size reduces to less than a few hundred meters. In such cases, Turbulent Kinetic Energy (TKE) diffusion scheme is used (Skamarock 2008).

Mellor-Yamada-Nakanishi-Niino (MYNN) PBL Scheme which includes Turbulent Kinetic Energy (TKE) based local mixing, has been used here. Potential temperature of liquid water, θ_l and total water content q_w are used as thermodynamic variables. It is tuned to LES simulation database to overcome biases associated with underestimated TKE and insufficient growth of convective boundary layer. It has elaborate mixing length formulations to flexibly change behavior across the stability spectrum.

Here,

$$\theta_l = \theta - \left(\frac{\theta}{T}\right)\left(\frac{L_v}{c_p}\right) q_l$$

$$q_w = q_v + q_l$$

Mixing length is designed such that shortest length scale among, l_s, l_t, and l_b will dominate:

$$\frac{1}{l} = \frac{1}{l_s} + \frac{1}{l_t} + \frac{1}{l_b}$$

where, surface layer length scale, l_s is a function of the stability parameter (ζ = z/L; L is the M-O length):

$$l_s = \begin{cases} kz(1 + cns\zeta)^{-1} & if\ 0 \le \zeta \le 1 \\ kz(1 + \alpha_4\zeta)^{0.2} & if\ \zeta < 0 \end{cases}$$

and the turbulent length scale l_t is:

$$l_t = \alpha_1 \frac{\int_{z=0}^{PBLH} zq\ dz}{\int_{z=0}^{PBLH} q\ dz}$$

and the buoyancy length scale l_b is:

$$l_b = \alpha_2 \frac{q}{N}\left[1 + \alpha_3\left(\frac{q_c}{l_t N}\right)^{1/2}\right]$$

where q_c is a turbulent velocity scale ~ O(w_*) .

Wind Farm Parametrization scheme

Combination of various key atmospheric parameters are used in simulating wind power. It can be estimated by the product of wind speed cube and rotor disc area, where power produced is in Watts (Jaramillo 2004).

$$P = \frac{1}{2}\rho A U^3$$

Wharton (2010) disproved theory stating that wind speed at rotor hub height gave exact value for calculating average wind speed through the rotor disc. They proved atmospheric stability that varies vertically had a significant effect on wind power production. All wind turbines have a maximum rated power output attained only at specific conditions. Since it is not possible to have a sustained rated output, we relate it with the generated power using capacity factor, CF (Jaramillo 2004).

$$CF = \frac{P}{P_R}$$

Power generated can be calculated using the above equation or from the power curves provided by the manufacturer. Wind turbines in U.S. have a maximum CF of 48 percent and annual CF of 35 percent (Wiser 2009). As accurate prediction of atmospheric dynamics lead to better wind power forecasting, wind farm modeling systems are used to evaluate the model.

Planetary boundary layer needs to be coupled with wind farm parametrization scheme to achieve higher accuracy. The differences occurred during comparison of simulated and observed condition are caused by averaging time and volume (Hanna 2001).

Power output curve is used to develop horizontal wind components using specific momentum tendencies which is a function of wind speed at rotor hub height. Power output P can be related to kinetic energy flow through rotor area.

$$P(\vartheta_{rh}) = C_p \frac{\rho_{lo}}{2} \vartheta_{rh}^3 \frac{\pi}{4} d_r^2$$

Where C_p= total efficiency coefficient

ρ_{lo}=reference air density (1.225 kg m^{-3})

ϑ_{rh}= wind speed at rotor hub

d_r= diameter of the rotor

C_p can be written as $C_p = C_a \eta_{elmech}$. C_a, where C_a is efficiency of harvesting kinetic energy flow through rotor area. For modern turbines, C_a varies from 0.45 to 0.55. Loss

factor η_{elmech} is caused due to friction by mechanical components and electrical circuits and this ranges from 0.85 to 0.95.

f(x,y) is the horizontal area density function of wind turbines. It does not vary in a grid box, hence it can be written as $f_{i,j}$, where i and j are grid indices.

Circle segment area integrals I (z_a, z_b) are:

$$I(z_a, z_b) = \int_{z_a}^{z_b} \int_{0}^{\sqrt{R^2-(z-z_{rh})^2}} dx\, dz$$

$$= \frac{R^2}{2}\left[arccos\left(\frac{z_a - z_{rh}}{R}\right) - arccos\left(\frac{z_b - z_{rh}}{R}\right) + \left(\frac{z_b - z_{rh}}{R}\right)\sqrt{1-\left(\frac{z_b - z_{rh}}{R}\right)} - \left(\frac{z_a - z_{rh}}{R}\right)\sqrt{1-\left(\frac{z_a - z_{rh}}{R}\right)}\right]$$

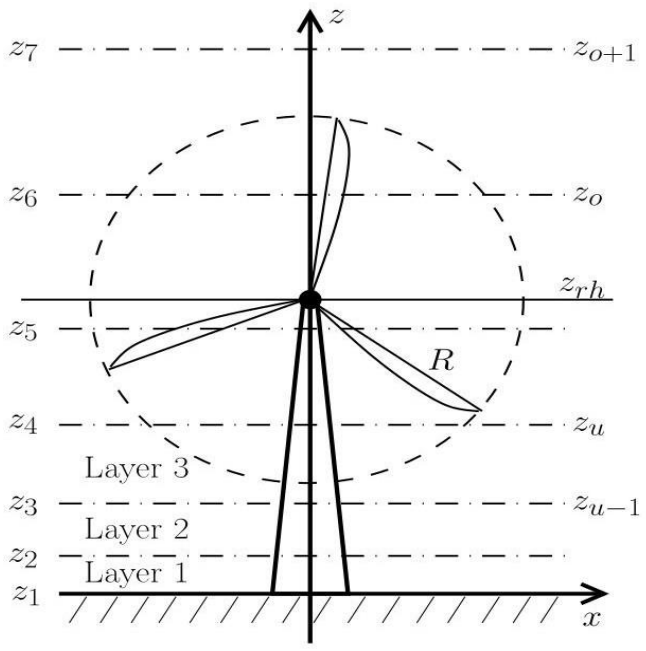

Figure 2.5. Wind turbine with vertical grid configuration. At hub height it is z_{rh} with Rotor radius R. (courtesy Blahak 2010)

In a grid box, the notation used for coordinate system is Cartesian model, with spatial coordinates as x, y, z and its corresponding velocity components as u, v, and w. Here x and y are horizontal, and z is the vertical coordinate.

Therefore, total kinetic energy within the volume of atmosphere that encloses a turbine is given as follows:

$$\dot{E}_{kin,pc}|_{wp} = -\frac{P(\vartheta_{rh}) f_{ij} \rho_{rh} \Delta x \Delta y}{\rho_{lo} \eta_{elmech}}$$

There is new parameterization scheme which has been developed called Fitch Parameterization Scheme in mesoscale model WRF for numerical weather prediction. This is the current scheme utilized throughout this research for resolving effects of wind turbines by imposing a momentum sink on the mean flow. This sink is implemented by transferring the kinetic energy to electricity and turbulent kinetic energy (TKE). It improves upon other schemes by basing aerodynamic drag on the modern commercial turbine's thrust coefficient. In addition, the TKE source varies with change in magnitude of the wind speed which reflects amount of energy extracted from the atmosphere by the turbines that do not have an electricity output.

The Fitch parametrization Scheme, which is an adaptation from Blahak et al, is used here. Wind turbines in this parametrization are treated as a density function. Upstream velocity experienced by turbines in the farm will be equivalent to the grid-cell velocity.

Turbulent fluxes in the momentum are:

$$\tau \equiv \rho u_*^2 = \rho C_D U^2$$

Where, p= air density

U = horizontal wind speed

C_D= drag coefficient

Turbulent kinetic energy is calculated for entire wind farm using the formula given below:

$$T_k = \frac{C_t N_{ij} A_k v_{h.k}^2}{2(\Delta x)^2 \Delta z_k}$$

Where, $N_{i,j}$= number of turbines in grid cell (i,j,),

$A_{i,j}$=Turbine blade segment intersecting with model level k,

Δx = horizontal grid spacing,

$v_{h,k}$= horizontal velocity

In addition to increased shear, turbulent kinetic energy will also have an additional source proportional to the cube of wind speed. In the model, qke = $u_i'^2$, i =1, 2, 3 (Fitch 2013)

$$qke_{(model+wake)} = qke_{(model)} + \alpha \frac{N_{ij} A_k v_{h,k}^3 \Delta t}{(\Delta x)^2 \Delta z_k}$$

where $\alpha = C_t - C_p$.

CHAPTER 3

MODEL SETUP

Selection of Domain

To extract maximum output, wind farms are installed in regions with high wind speeds. Domain for this research was selected based on the data provided by NREL. Figure 1.1 shows annual average wind speed over United States at a height of 80 m. It can be concluded from the chart that south of Oregon and northern part of California receive highest coastal wind speeds of more than 10 m/s. Wind farms in the current model have been placed in region with highest wind speed.

Domain for this research was placed over South Oregon, bordering California. The domain selection was done using WRF Domain Wizard provided by Earth System Research Laboratory (NOAA).

The outermost domain, namely domain 1, has a grid spacing of 25000m both in x and y direction. Domain 2, which is inside domain 1 has a finer grid spacing of 5000m and the innermost domain, domain 3, has the finest grid spacing of 1000m in both x and y directions.

The outermost domain has an area of 373750 km^2, domain 2 has an area of 47275km^2, and the inner most domain has an area of 5551km^2. The domains selected are in such a way that there is equal land mass and ocean area for installation of onshore and offshore wind farms. Table 1.1 gives the configuration of each of the domains used for this research.

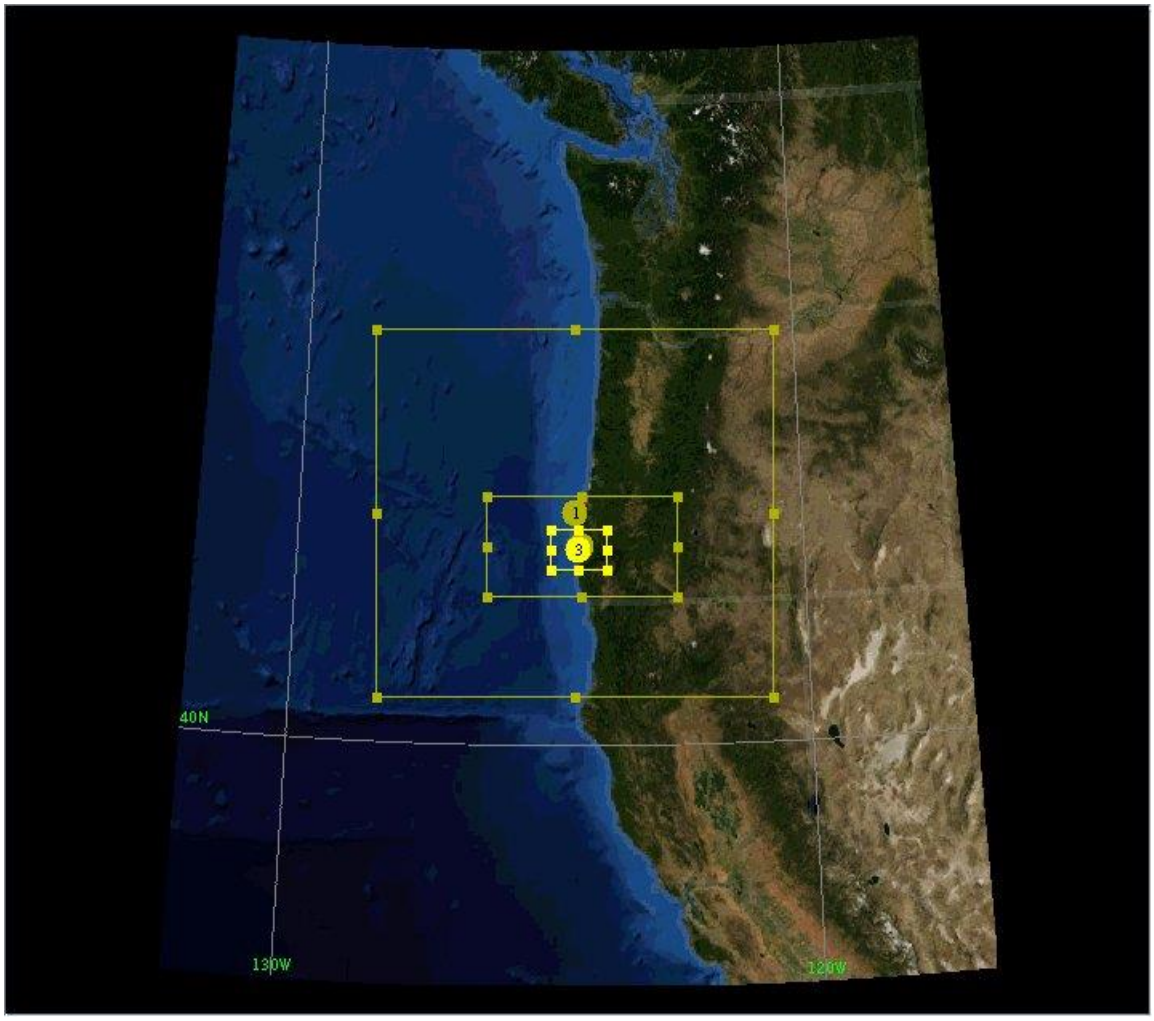

Figure 3.1. Projection of domain generated sing WRF Domain Wizard

Table 3.1. Domain configuration

Domain	Resolution	Length x axis	Length y axis
3	1 km	90 km	60 km
2	5 km	300km	150 km
1	25 km	650 km	575 km

Wind Turbine selection and placement

Until now, wind turbines used in research studies conducted by Fitch et al 2012, Adams et al 2013 and other researchers, include a maximum turbine power of 3 to 4 MW and are spread over large areas. With the onset of new technology onshore turbines have reached power outputs of 7.58 MW and offshore turbines have attained 8 MW.

Enercon E-126 (7.58 MW) and Vestas V-164 (8 MW) are commercially available and are being manufactured on a full scale. Vestas V-164 was made only to be used for offshore purposes, whereas Enercon E-126 can be used for both onshore and offshore purposes. In this study, location and placement of the wind farm is varied, therefore, Enercon E-126 has been chosen. Table 3.1 give the specifications of Enercon E-126. Figure 3.2 is a picture of an actual Enercon E-126, installed in Germany.

Table 3.2. Enercon E-126 Wind Turbine specifications (Courtesy Enercon)

Parameters	Specifications
Hub height	135 m
Turbine diameter	127 m
Cut-in speed	3 m/s
Cut-out speed	34 m/s
Rated Power	7.58 MW

Selection of Wind Farm size and its placement

The size of wind farms in this study are in conjunction with actual size of the wind farms, so that results obtained can be related to real time cases. Research conducted

until now was based on a power density of 4 Wm^{-2} and with farm sizes of 100 x 100km. This research has considered a power density of 7.58 Wm^{-2} with farm size of 30x30 km.

Figure 3.2. Enercon Wind Farm installed in Georgsfeld near Aurich, Germany (courtesy: http://www.volkswind.us/wind-farms/reference-wind-farms.html)

Two simulations were run, one for onshore and the other for offshore. Simulations were run for a period of 31 days for the month of January, and 31 days for the month of July. Simulations were also done without any wind farm to obtain a benchmark for comparison.

The atmospheric data was used from year 2010. It was obtained from National Center for Atmospheric Research, which uses .fnl format having a time stamp with respect to Greenwich Mean Time (GMT).

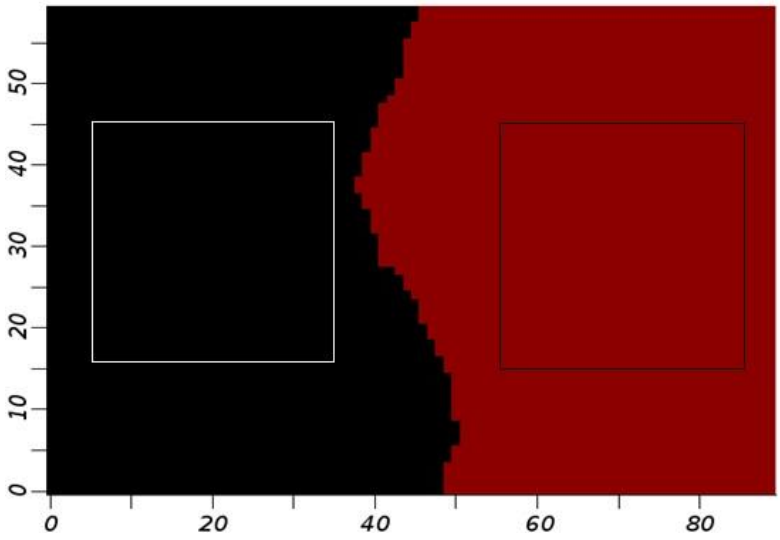

Figure 3.3. Domain 3, innermost domain, brown color represents land and black represents ocean

Farm was placed in innermost domain (domain 3), which has the highest resolution with grid spacing of 1km.

Figure 3.3 shows two outlines, the one on land represented by a red background is the size of onshore wind farm and one with a black background over the ocean, is offshore wind farm.

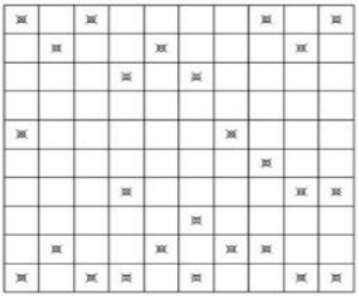

Figure 3.4. Mosetti et al' optimal layout (courtesy Mosetti 1994)

Unlike optimal layout designed by Mosetti et al, Marmidis et al or genetic algorithm, the wind turbines are placed in a square shape where each turbine is equidistant from one another in directions north, south, east or west, but not diagonally.

When wind turbines are placed in a farm, there are inevitable power losses because of turbulence produced by other turbines within the farm. Average power losses are in range of 10% to 25% (Yu-ting 2015). Breakdown of the vortex produced by a wind turbine is also important as it reduces turbulence in air, so that turbines situated downstream produce sufficient power with lower loses.

Vortex breakdown as observed by Troldberg (2007) was between 1.5D to 2.5D from the turbine. For a uniform flow, wake of the vortex was found to be much longer, about 5 times the diameter, before it starts to breakdown (Harish 2014).

Since wind turbine spacing is important, the general thumb rule is that, two consecutive wind turbines should have a distance of at least 5 to 15 D between them. The diameter of turbine used here is 127m and distance between the turbines is 1km. Therefore the distance in terms of diameter is 7.87 D, which is neither too far nor too close and can be considered a reasonable distance for the vortex breakdown.

Since the topographical region around an onshore wind farm is not exactly flat, i.e. it might have a terrain filled with hills roughly the same height as the wind turbines, there would be a boost in wind speed to turbines in certain areas of farm. This occurs due to relative increase in its height from sea level. On the flipside, there might be wind turbines within the farm which get lower wind speeds due to the obstruction caused by the topology.

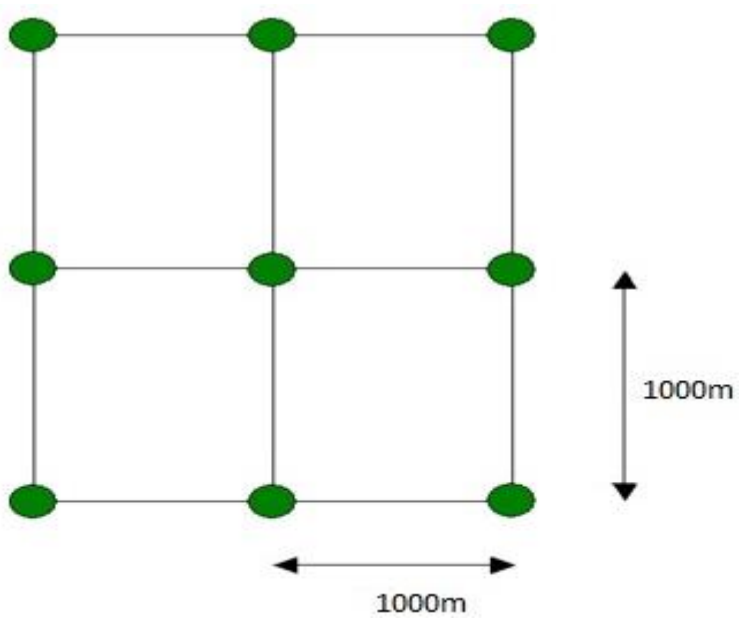

Figure 3.5. Wind turbine spacing in both offshore and onshore wind farm

The offshore wind farm is placed over ocean such that effects of terrain is barely observed. As the friction is much lower over water bodies, wind speeds are fairly consistent.

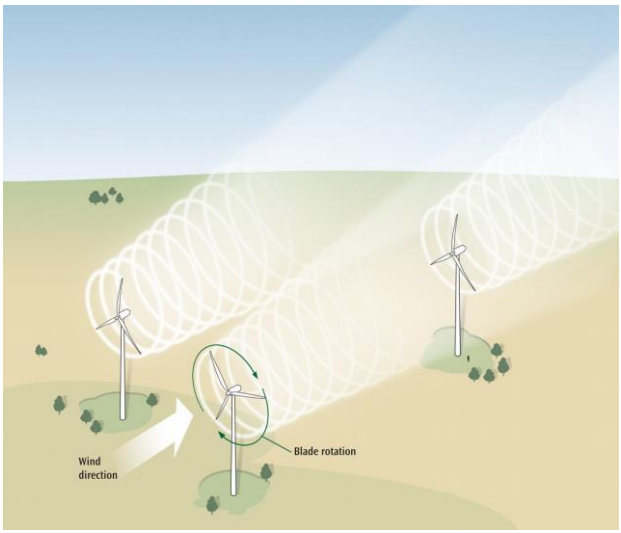

Figure 3.6. Wind turbine vortex formation (Courtesy: http://energy.sandia.gov/energy/renewable-energy/wind-power/scaled-wind-farm-technology-swift-facility/)

CHAPTER 4

RESULTS AND DISCUSSION

Offshore and onshore effect on local weather

For present research simulation, weather data was used for the month of January and July from year 2010. This provides 31 days each in different seasons to study the change in local weather around wind farms. Weather data was taken from NCAR, which provides data in final format (.fnl). Each file has atmospheric data for 6 hours and hence there are 4 files per day. This data provides for significant boundary conditions required to study weather for a particular region.

To avoid discrepancy, the time for each file is in conjunction with Greenwich Mean Time (GMT). Since the state of Oregon has been considered for this research, there is a difference of 7 hours, which is considered while converting to local time. As stated earlier, each wind farm has 900 wind turbines placed 1 km apart from each other in a square format and over an area of 30km X 30km.

For results generated, time averaging was done to analyze weather during day and night for the months of January and July. This is done to minimize any perturbations that might have been caused by bad weather for a day or two.

Results were recorded at a time interval of 3 hours to reduce size of the output file. This also helps while working with these files in MATLAB for post processing. For results generated for daytime in simulation, recording intervals are 10am, 1pm and 4pm. For night time in simulation, the recording intervals are 10pm, 1am and 4am. Time

averaging plots are generated at these times for day and night. A gap of 12 hours clearly defines the difference between day and night for post processing analysis.

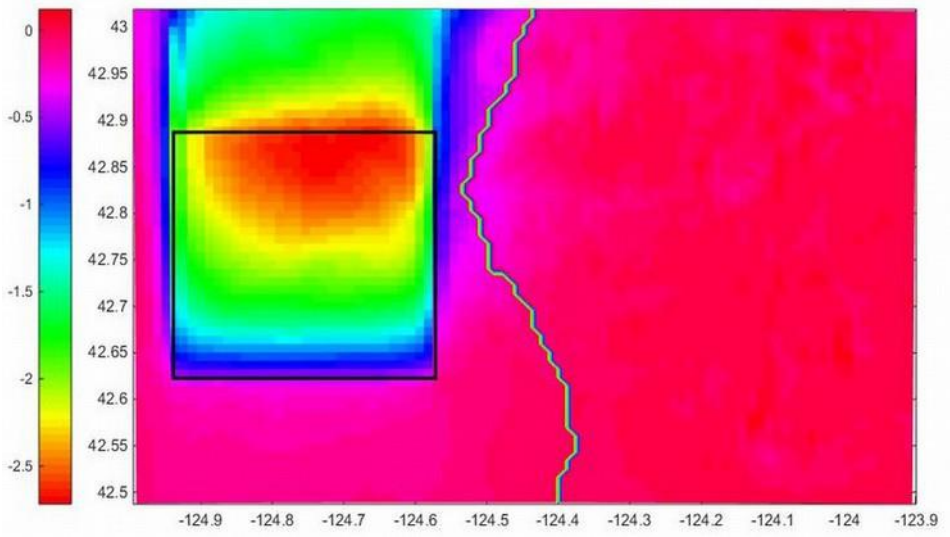

(a)

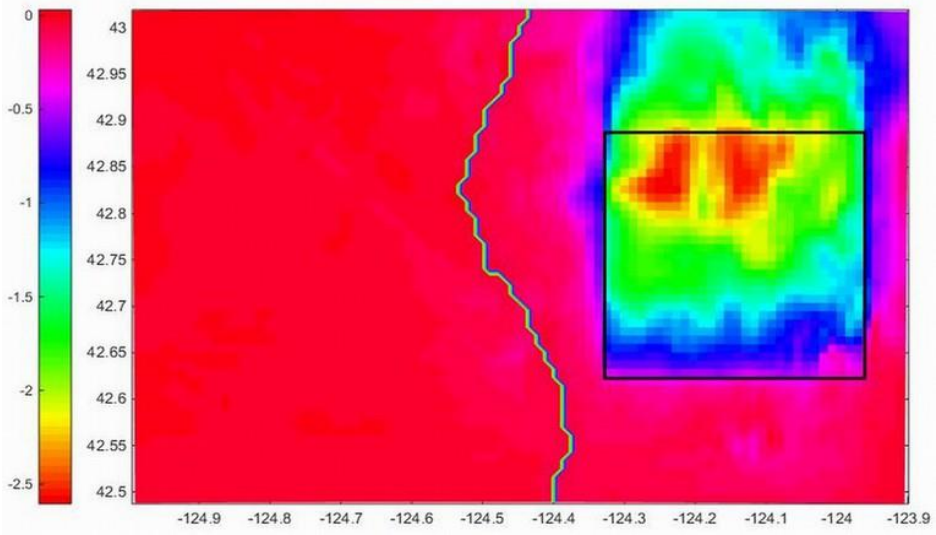

(b)

Figure 4.1. Mean velocity difference at 150m during time averaged day in Jan for (a) offshore vs no farm, (b) onshore vs no farm

Since the turbine hub is at a height of 135 m and the rotor diameter is at 127 m, total turbine height is 198.5 m. Mean velocity is calculated at 150m above the ground to

check for correctness of simulations. Results generated agreed with the fact that velocity of wind reduces due to wind farms.

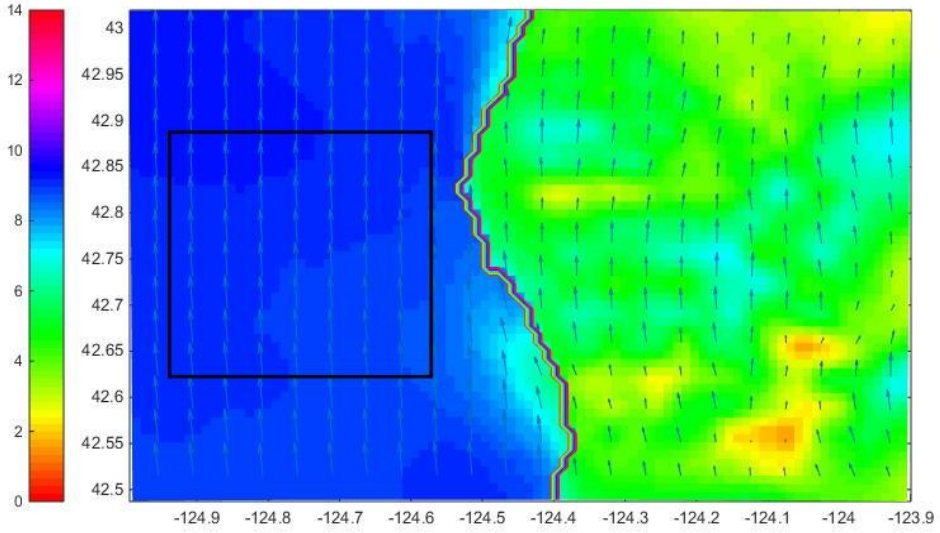

(a)

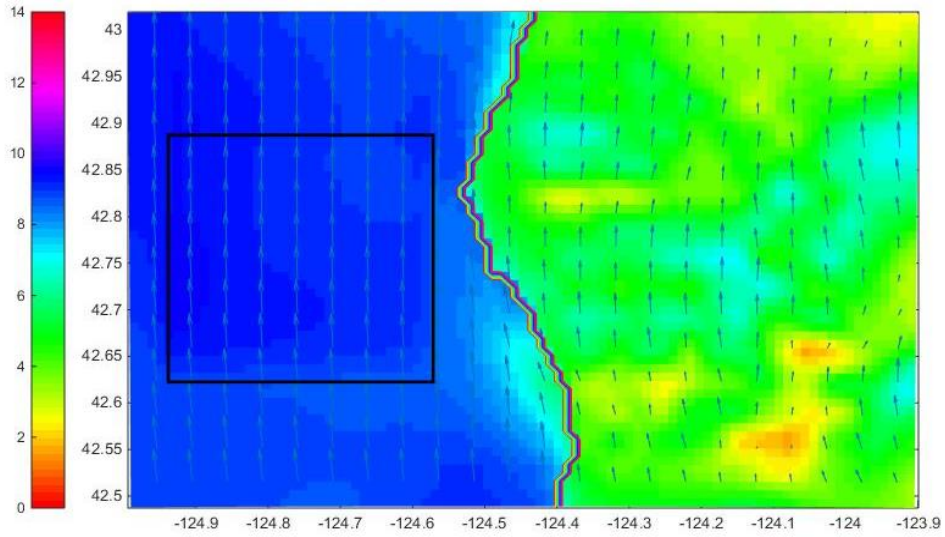

(b)

Figure 4.2. Velocity at 10m height during time averaged day in Jan for condition of (a) no farm, (b) offshore wind farm

The difference in mean velocity was calculated by subtracting the mean velocities with and without wind farm. The difference is same for onshore and offshore wind farms, at a height of both 10m and 150m.

From the figure 4.3, it can be seen at 10m height, there is a subtle increase in overall local wind velocity. Such increase contradicts velocity reduction at 150m.

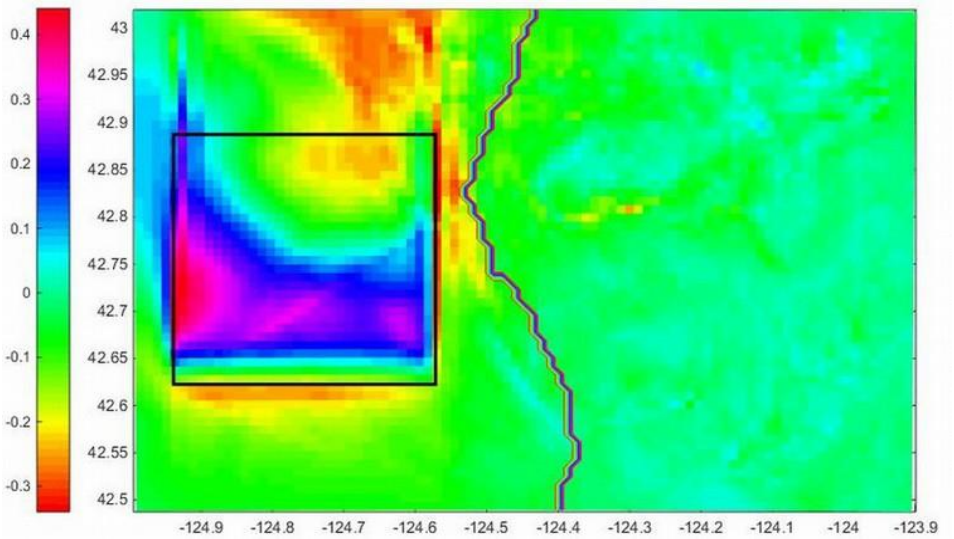

Figure 4.3. Mean velocity difference between offshore and no wind farm at 10m altitude for time averaged day in Jan

Even though the velocity difference is taken as 'wind farm' minus 'no wind farm', mean velocity plot reinforces our earlier interpretation at 10m, i.e. average wind velocity is increasing inside the wind farm.

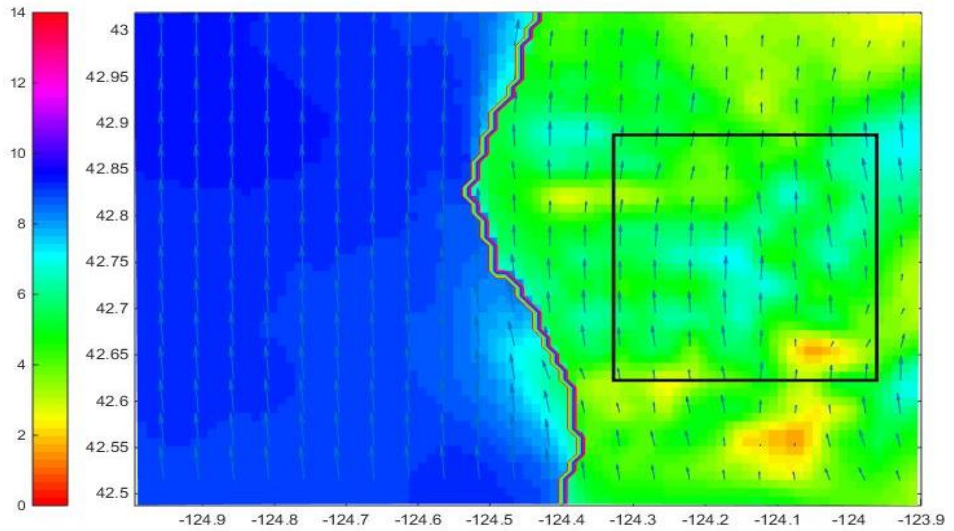

Figure 4.4 (a). Velocity at 10m height during time averaged day in Jan for condition of no farm

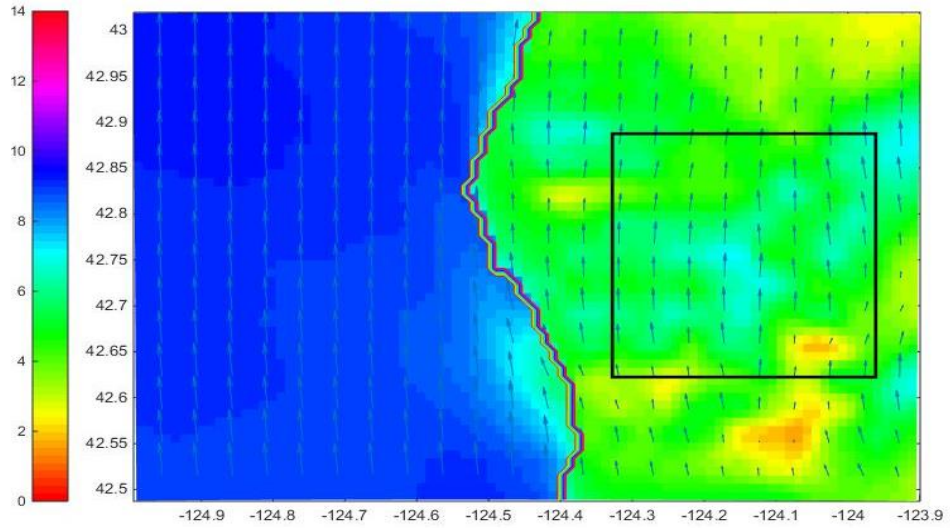

Figure 4.4 (b). Velocity at 10m height during time averaged day in Jan for condition of onshore wind farm

It can be observed from plots in figure 4.4, that even onshore wind farm has caused an overall increase in wind velocity at 10m. From figure 4.5, it can be observed that increase is higher in onshore wind farms compared to offshore wind farms of same size and power.

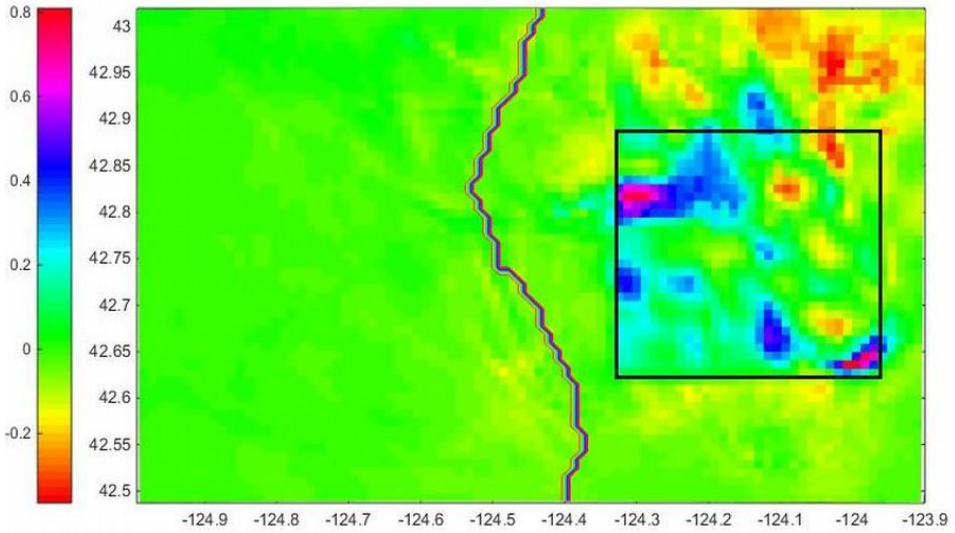

Figure 4.5. Mean velocity difference between onshore and no wind farm at 10m altitude for time averaged day in Jan

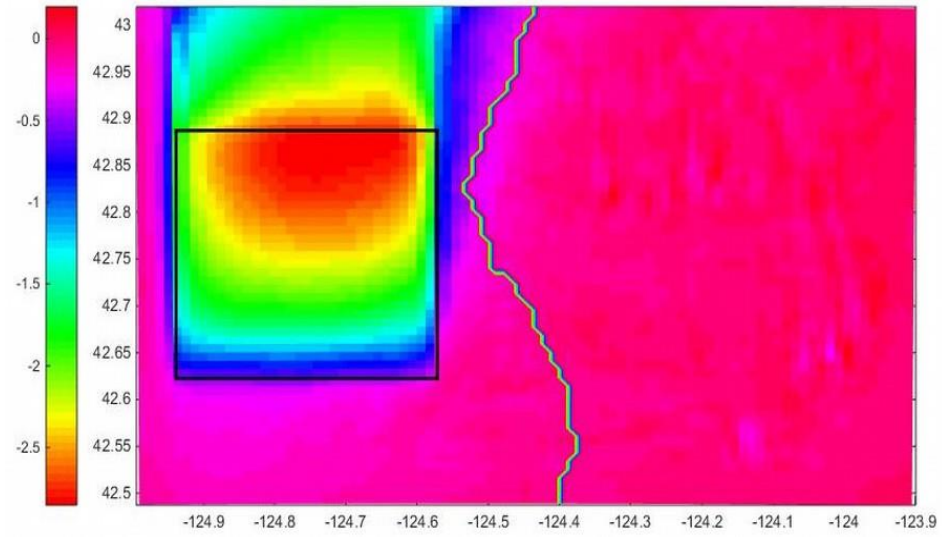

(a)

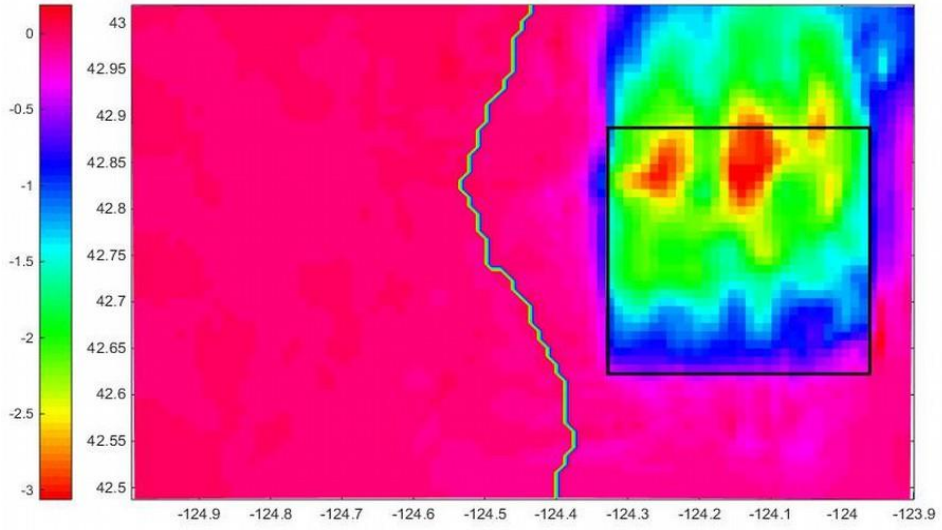

(b)

Figure 4.6: Mean velocity difference at 150m during time averaged night in Jan for (a) offshore vs no farm, (b) onshore vs no farm

During night it can be observed that mean velocity difference is comparatively higher than day.

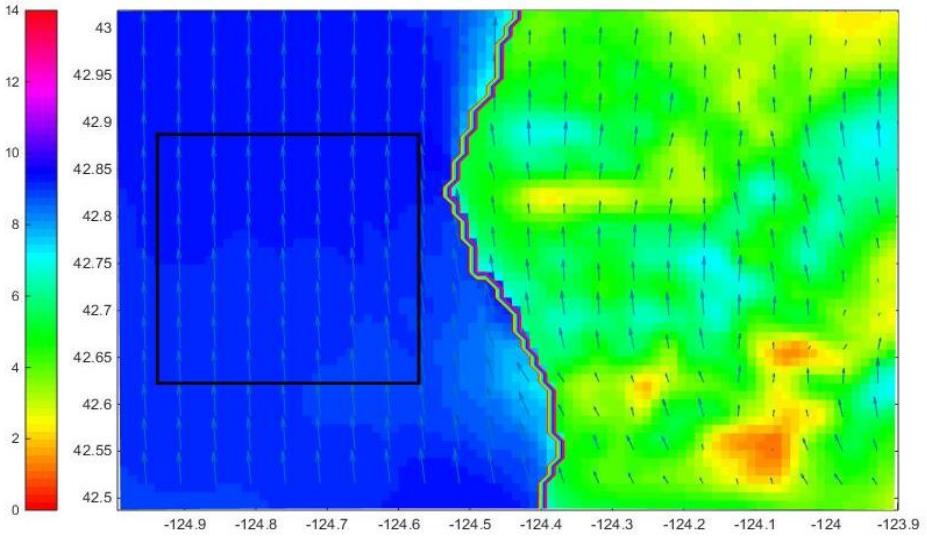

(a)

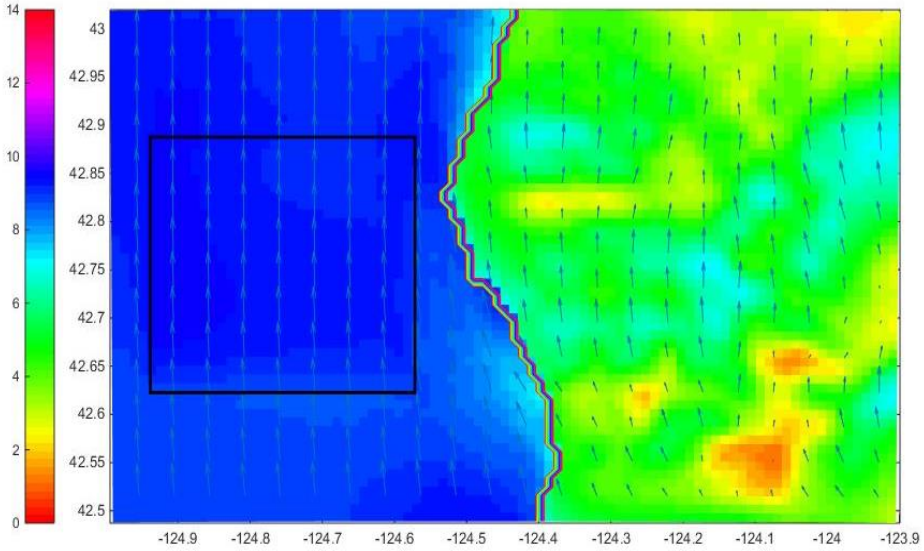

(b)

Figure 4.7: Velocity at 10m height during time averaged night in Jan for condition of (a) no farm, (b) offshore wind farm

Due to installation of offshore wind farm, there is a slight change of direction in the wind. In no farm condition the wind can be seen flowing towards northwest, while with farm, it's flowing directly towards north, as if wind turbines have channelized the flow.

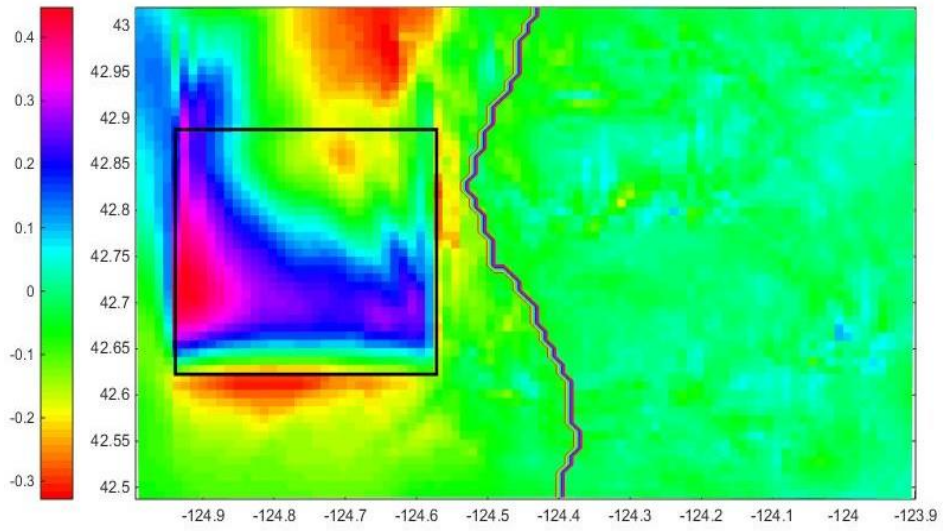

Figure 4.8. Mean velocity difference between offshore and no wind farm at 10m altitude for time averaged night in Jan

In figure 4.8, an increase in wind velocity can be observed after installation of wind farm. For both day and night, increase in wind velocity was observed only to the west of the farm.

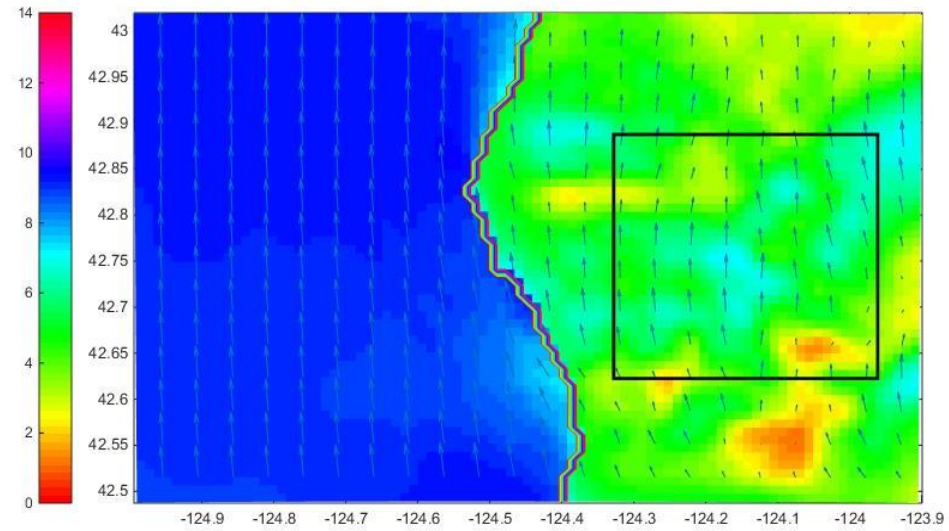

Figure 4.9 (a): Velocity at 10m height during time averaged night in Jan for condition of no farm

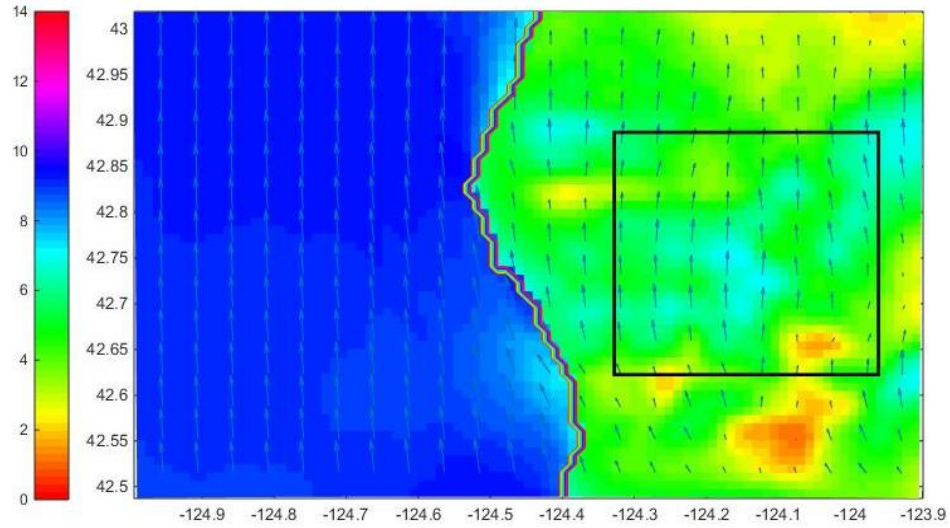

Figure 4.9 (b): Velocity at 10m height during time averaged night in Jan for condition of onshore wind farm

The onshore trends for night appear similar to that of day, both having an increase in local wind velocity due to wind farm. From the mean velocity difference plot in figure 4.10, it can be observed that wind velocity increases more during night than during the day time.

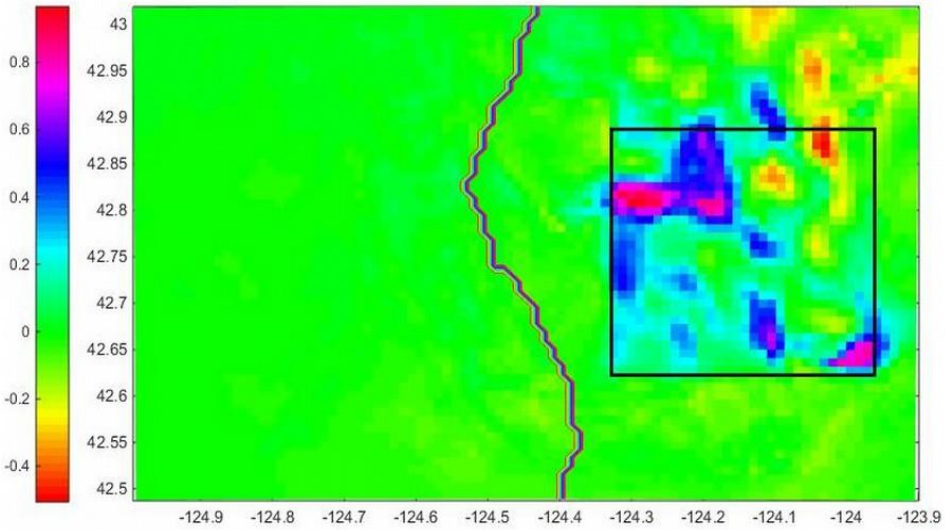

Figure 4.10. Mean velocity difference between onshore and no wind farm at 10m altitude for time averaged night in Jan

Seasonal effect on offshore and onshore wind farm

In order to get more conclusive results and to understand the underlying phenomenon, simulations were also conducted for the month of July. This would take into account the seasonal effect, which is considerable on such large scale wind farms.

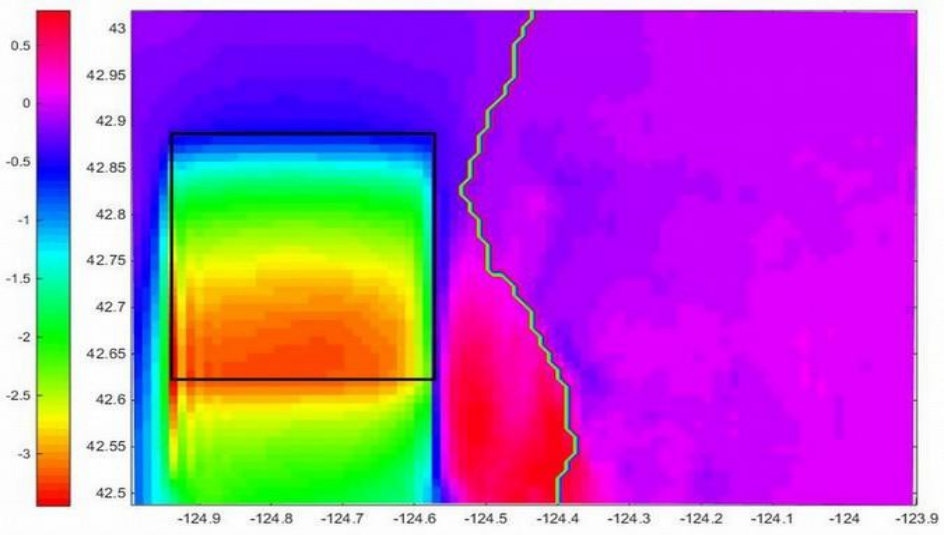

(a)

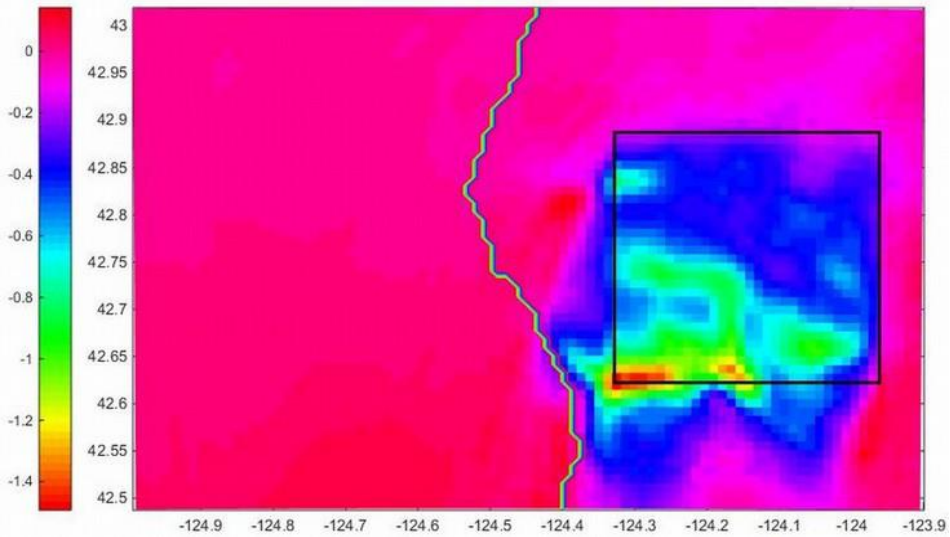

(b)

Figure 4.11. Mean velocity difference at 150m during time averaged day in July for (a) offshore vs no farm, (b) onshore vs no farm

As compared to onshore wind farms, for offshore wind farms, at a height of 150m, there is a tremendous change in mean velocity difference.

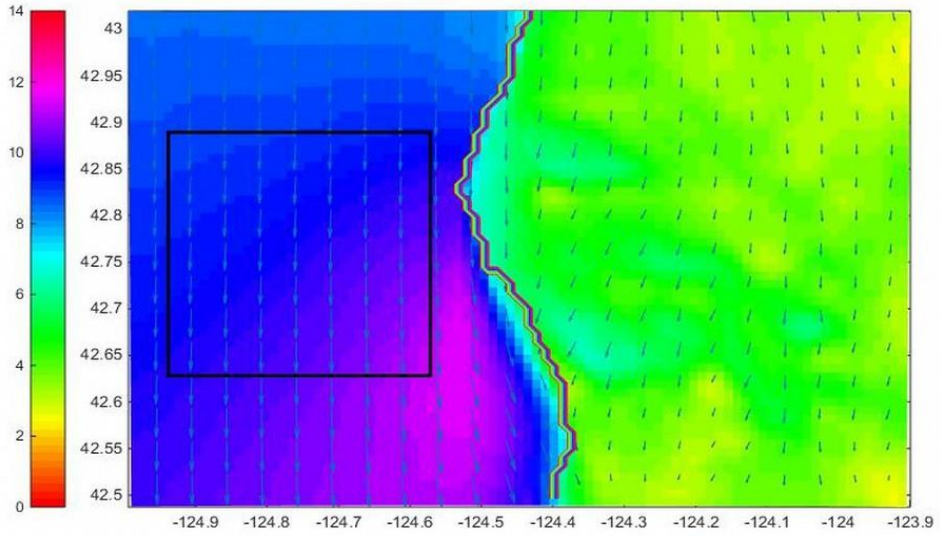

(a)

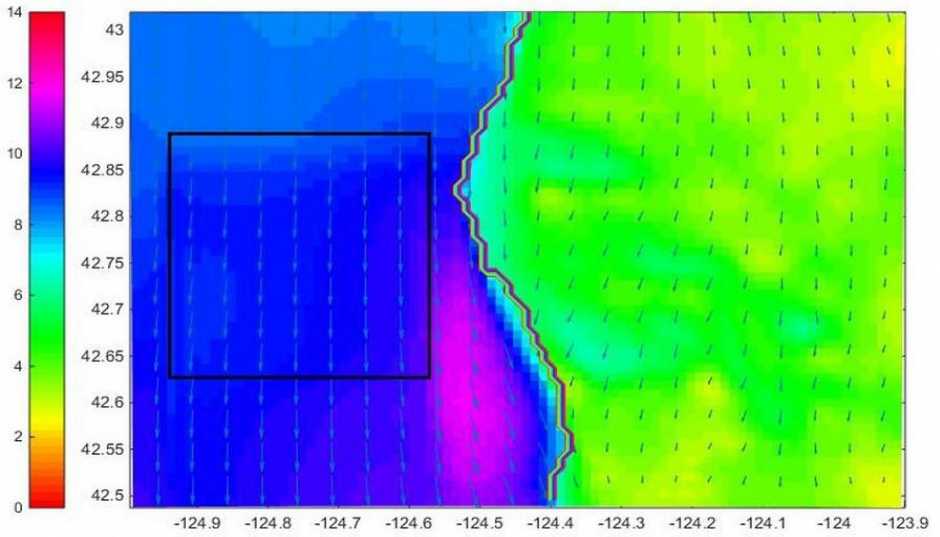

(b)

Figure 4.12. Velocity at 10m height during time averaged day in July for condition of (a) no farm, (b) offshore wind farm

In July, direction of wind is opposite to that of January. The installation of wind farm diverts the streamlined flow towards southwest, contrasting to that of January. It can also be observed that velocity reduces due to wind farm. In figure 4.13, mean velocity is

negative inside wind farm, which is in conjunction with the values at 150m altitude. Also to be observed, is a small part inside the farm, where local wind velocity increases.

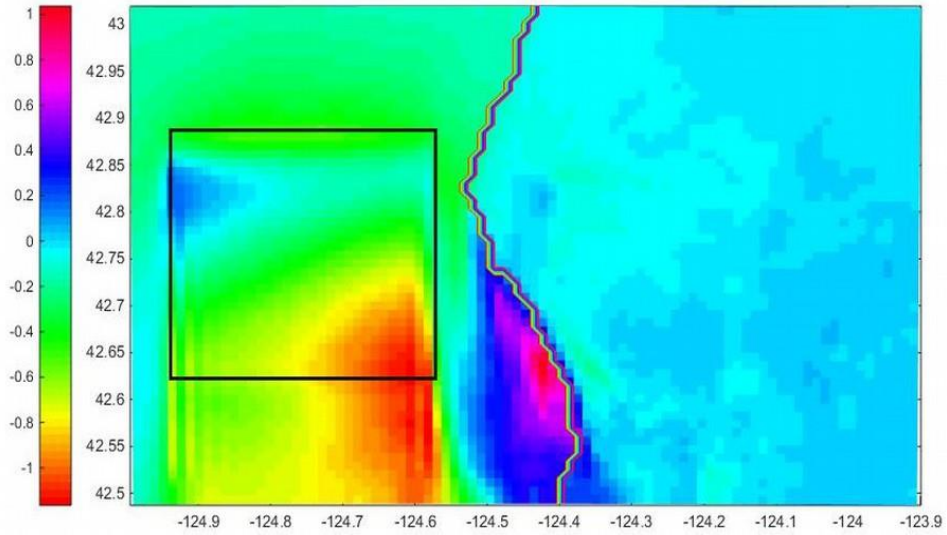

Figure 4.13. Mean velocity difference between offshore and no wind farm at 10m altitude for time averaged day in July

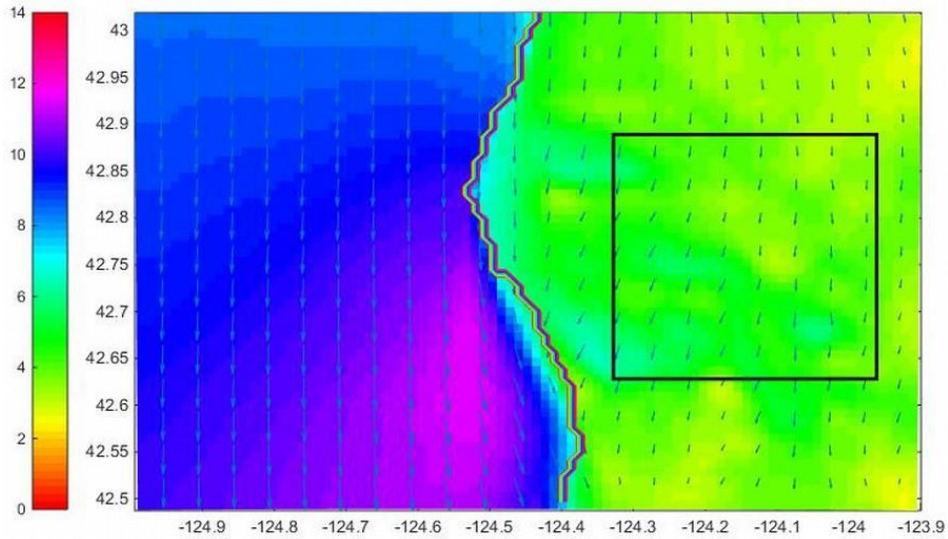

Figure 4.14 (a). Velocity at 10m height during time averaged day in July for condition of no farm

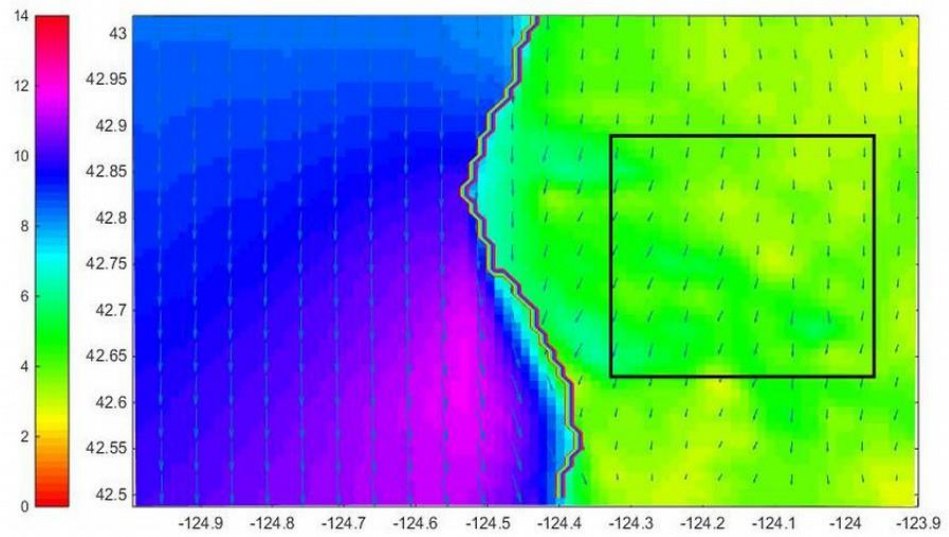

Figure 4.14 (b). Velocity at 10m height during time averaged day in July for condition of onshore wind farm

In case of onshore simulation, there is a reduction in wind velocity due to farm but no change in wind direction. The mean velocity difference plot shows a reduction of wind velocity throughout wind farm, and gradually increases towards the end of the farm.

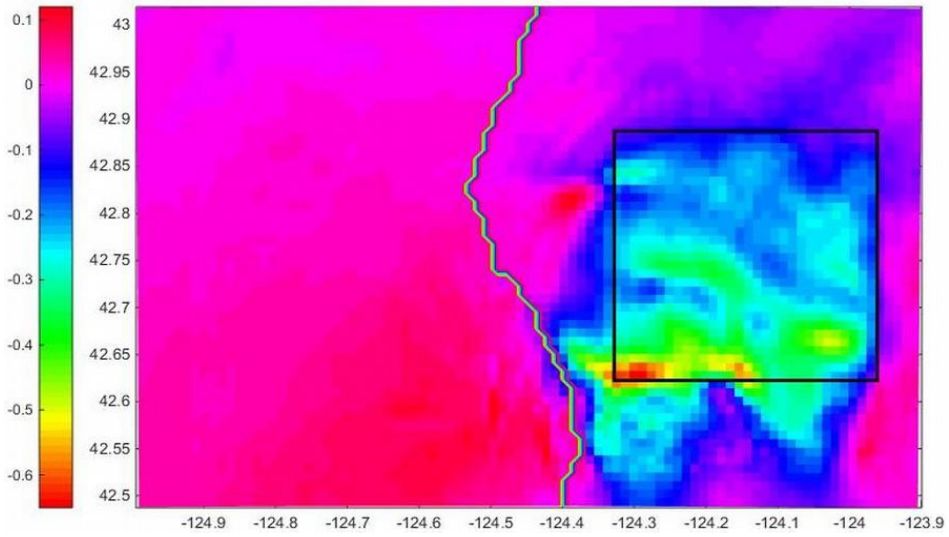

Figure 4.15. Mean velocity difference between onshore and no wind farm at 10m altitude for time averaged day in July

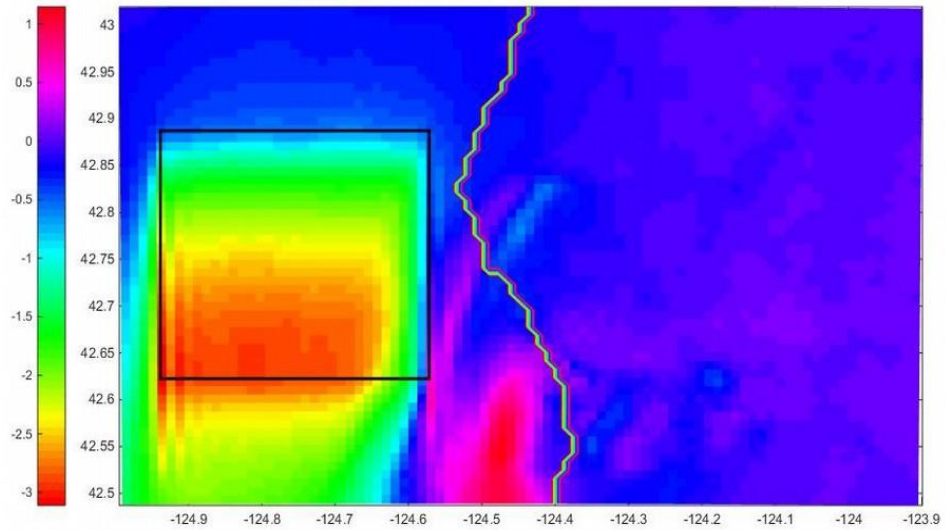

(a)

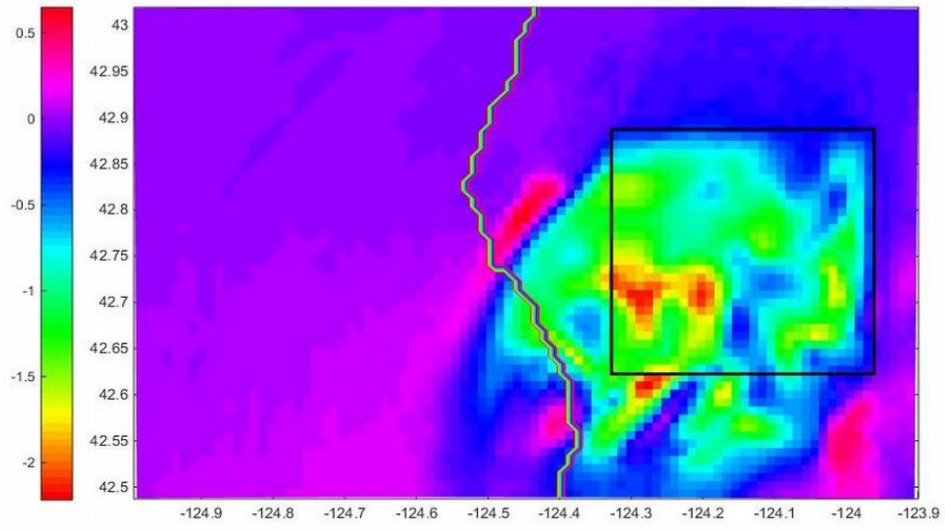

(b)

Figure 4.16. Mean velocity difference at 150m during time averaged night in July for (a) offshore vs no farm, (b) onshore vs no farm

The mean velocity difference at 150m shows a reduction in wind velocity, however, it has red spots outside the farm, indicating an increase in wind velocity. It can be deduced that direction of the wind is southwest.

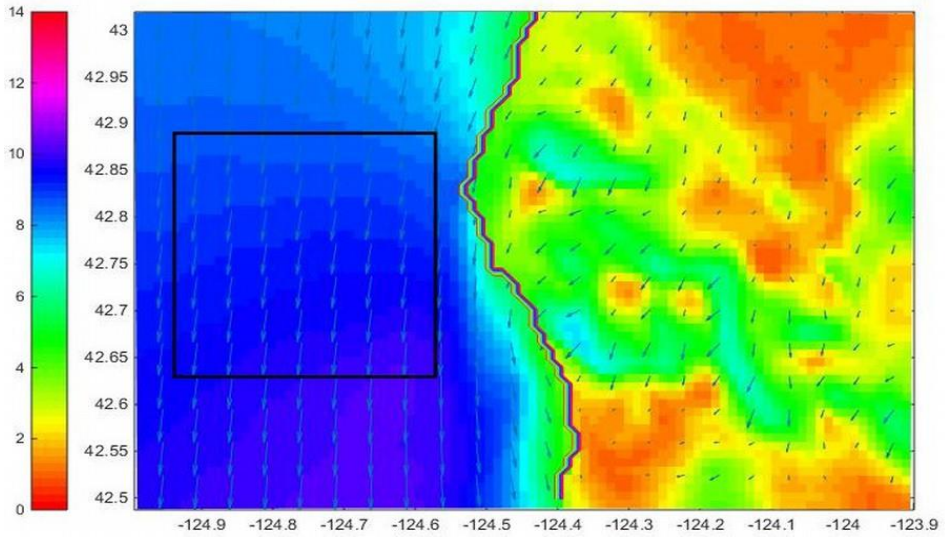

(a)

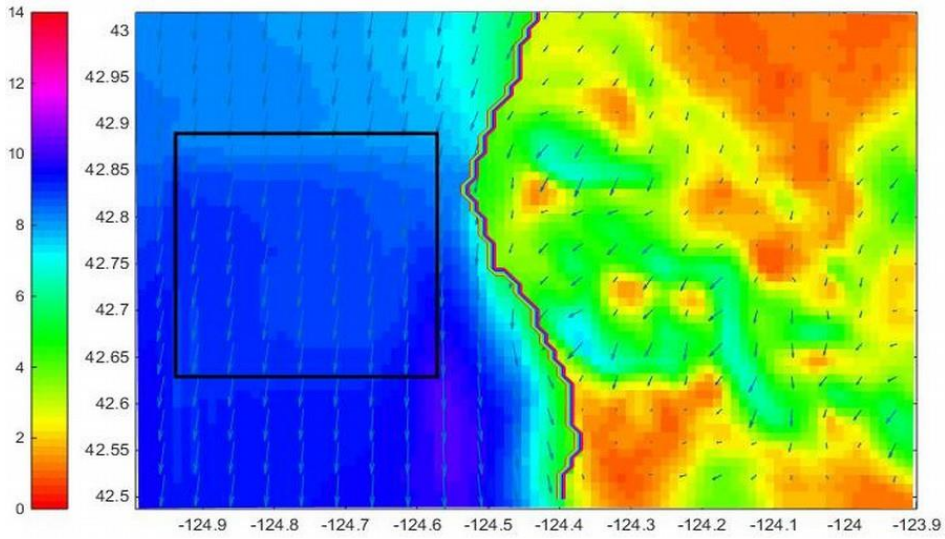

(b)

Figure 4.17. Velocity at 10m height during time averaged night in July for condition of (a) no farm, (b) offshore wind farm

Even though wind farms streamline the flow of wind, it can be observed that wind tends to flow towards southwest rather than south inside the farm. Mean velocity difference at a height of 10m shows observable changes in wind velocity throughout the farm with maximum difference at southern part.

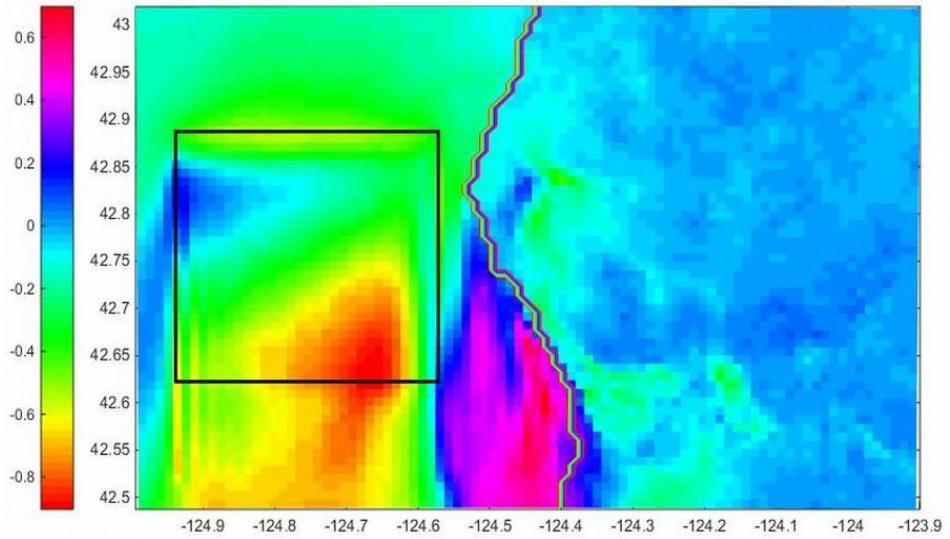

Figure 4.18. Mean velocity difference between offshore and no wind farm at 10m altitude for time averaged night in July

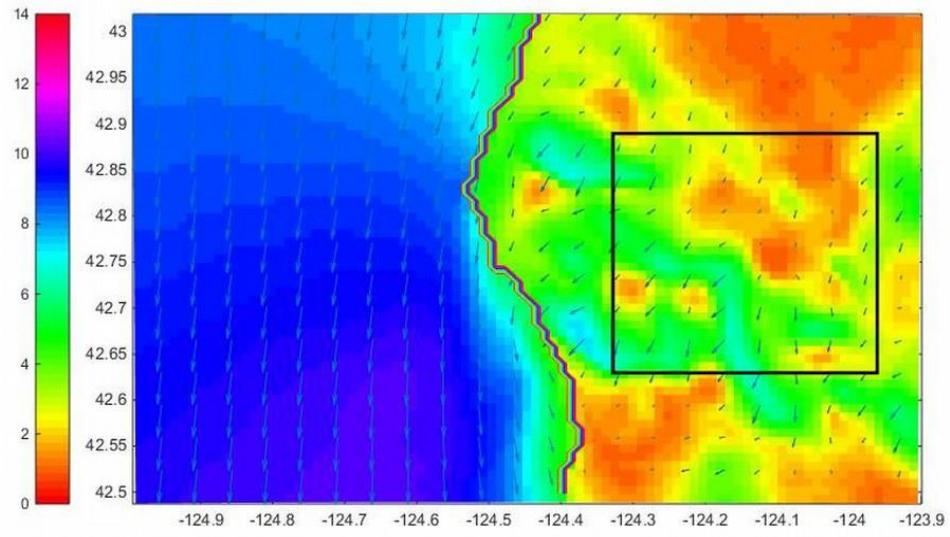

Figure 4.19 (a). Velocity at 10m height during time averaged night in July for condition of no farm

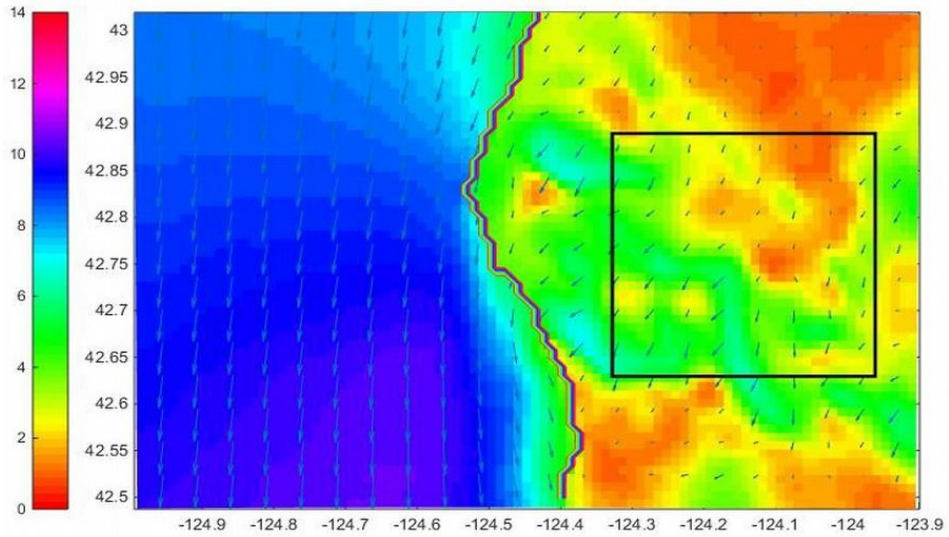

Figure 4.19 (b). Velocity at 10m height during time averaged night in July for condition of onshore wind farm

Unlike offshore wind farm simulation, there is no noticeable change in direction vectors throughout the farm for onshore conditions. Except for small regions inside the farm, where local wind velocity increases, there is a steady decrease in wind velocity.

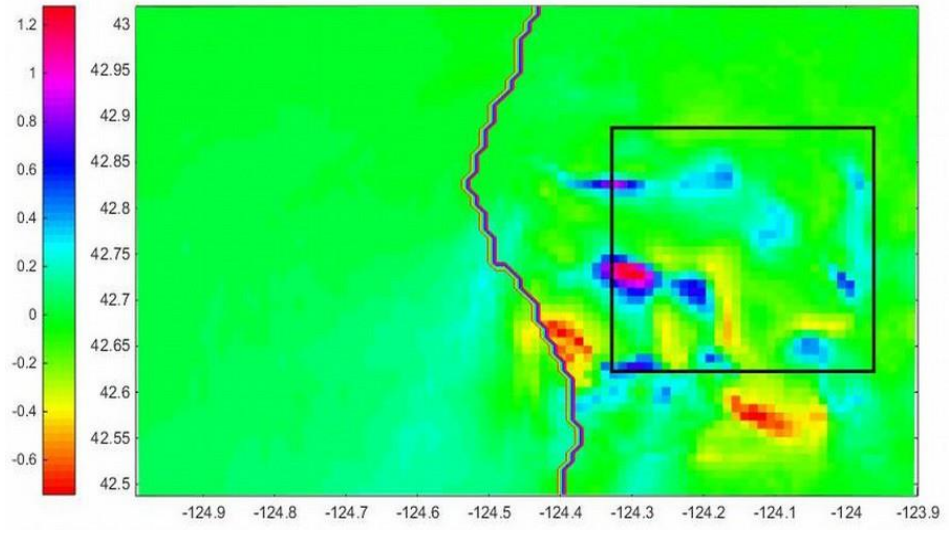

Figure 4.20. Mean velocity difference between onshore and no wind farm at 10m altitude for time averaged night in July

Comparison between offshore and onshore

Since wind is flowing either from north to south or from south to north with change in seasons, comparisons have been done on three different lines along north-south axis; top edge, middle line and bottom edge.

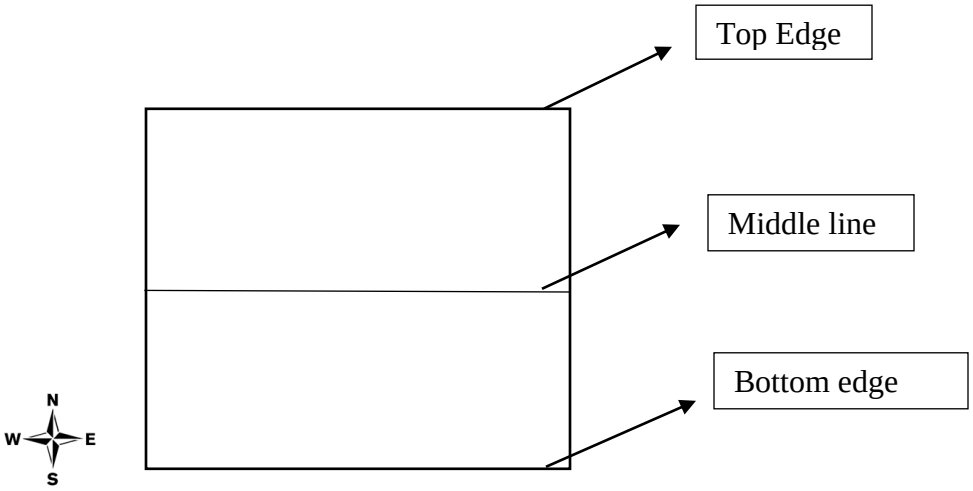

Figure 4.21. Representation of different lines along north-south axis

At each line velocity was plotted for both day and night. Directional change in wind from South to North in January and North to South in July was observed.

It can be noticed that there is a considerable change in velocity from offshore to onshore along the latitude. This is due to the fact that over ocean surface, friction is low and there are no obstacles for wind. But onshore, the friction is higher and there is obstruction due to change in topography.

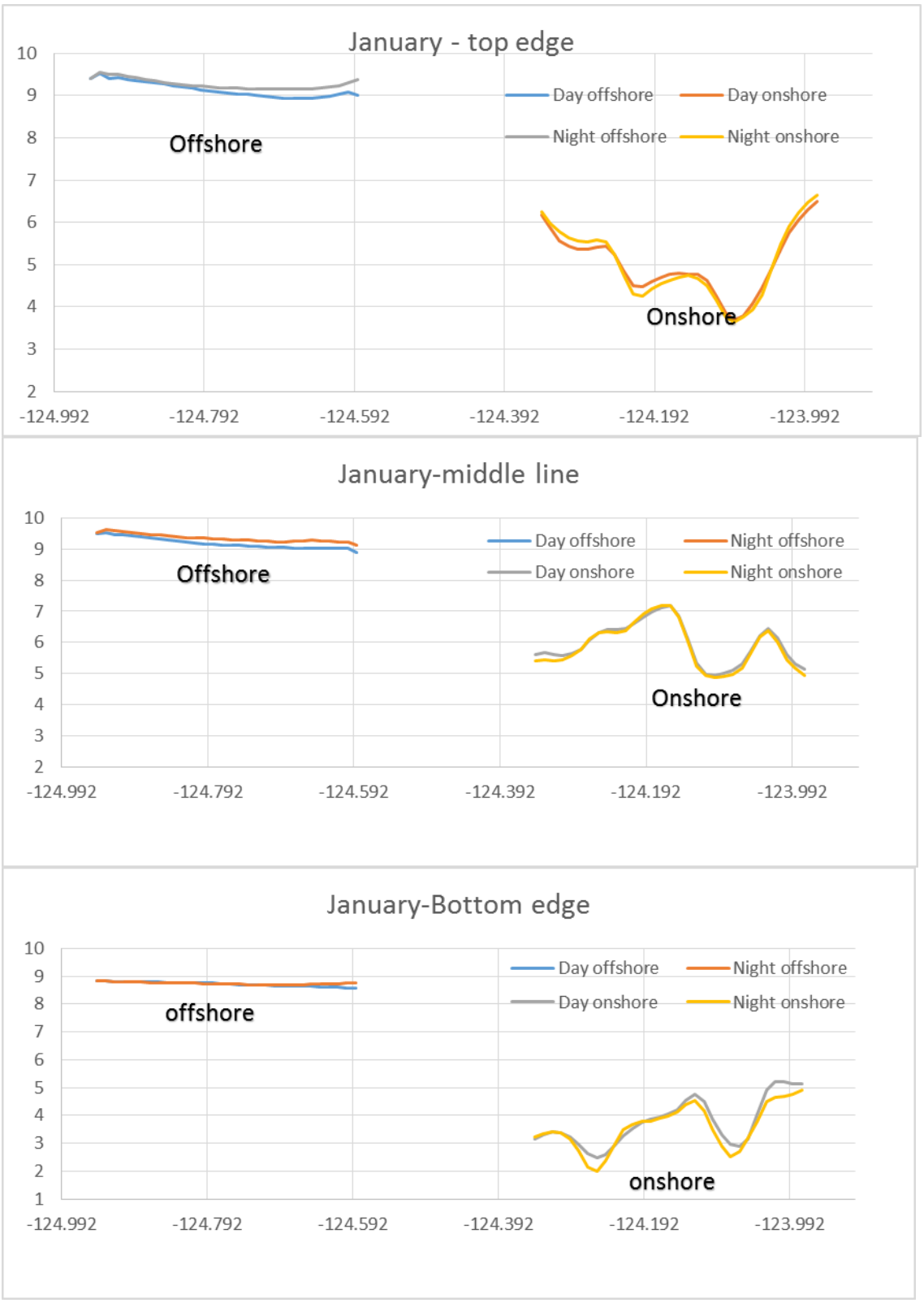

Figure 4.22. Graph between local wind velocity m/s (x-axis) and latitude (y-axis) for month of January

It can be referred from the figure 4.22 that for bottom edge, where wind first interacts with the wind farm, offshore case has barely any difference from day to night. For onshore though, the local wind velocity is lower by approximately 0.5m/s.

For middle line, velocity is higher during night for offshore than onshore, and the change is approximately 0.3m/s. For onshore there is hardly any noticeable difference in velocity from day to night.

For top edge, velocity trend for offshore is similar to that of middle line. For Offshore, the local velocity for top edge is higher than that for bottom edge. Whereas onshore, unsteady change along the latitude can be attributed to change in terrain, and hence the plots for day and night are overlapping. For both offshore and onshore, minor fluctuations were observed in wind velocity for day and night.

For month of July and at top edge of offshore wind farm, day and night has a difference in wind velocity of less than 0.5m/s on west side, gradually increasing to 1.5 m/s towards east side. Local velocity at night is reduced in comparison to day.

For onshore wind farm, the difference is noticeable, and is approximately 1.5 to 2 m/s from day to night. Reduction in velocity is observed both onshore and offshore with magnitude of reduction being higher onshore.

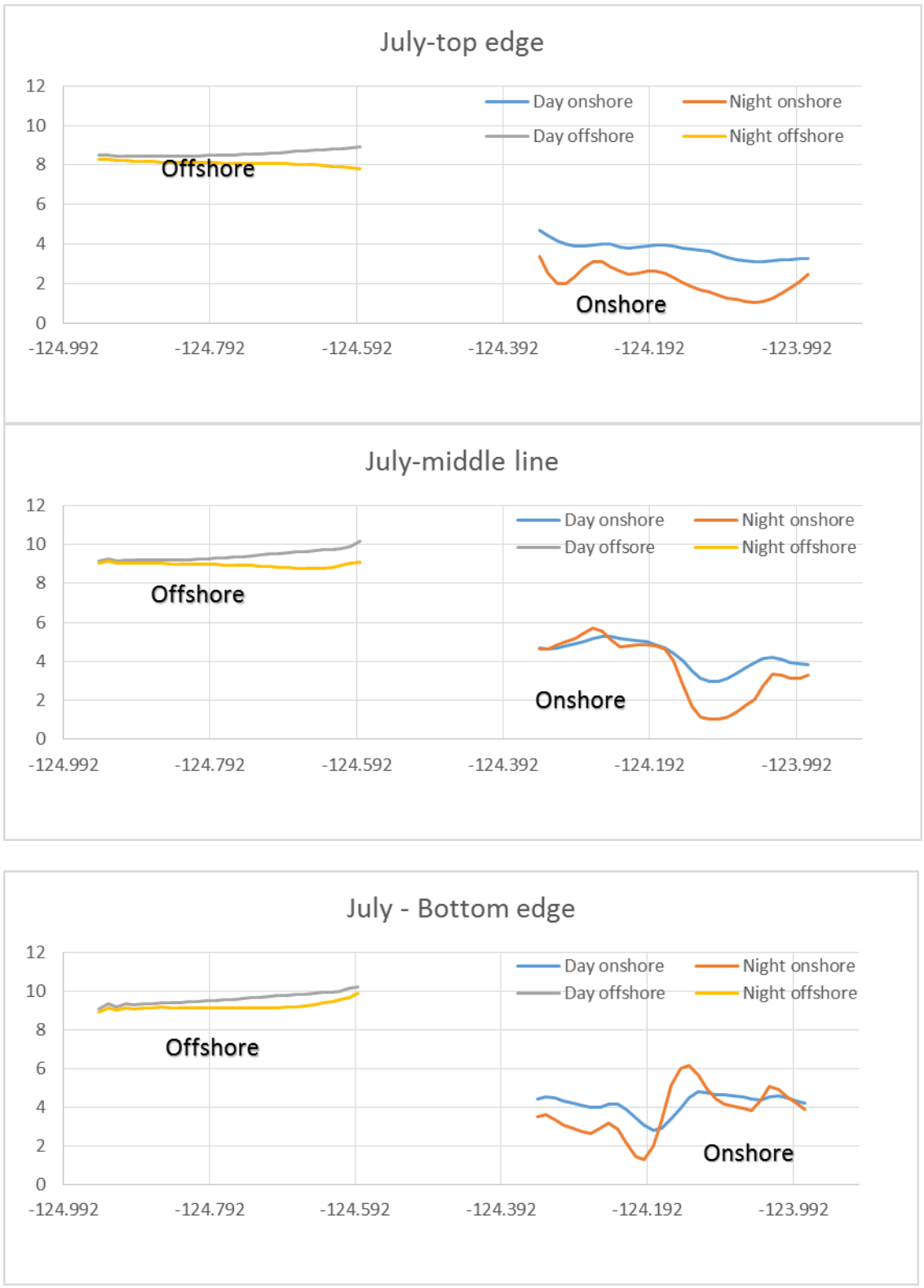

Figure 4.23. Graph between local wind velocity m/s (x-axis) and latitude (y-axis) for month of July

For middle line, the average velocity increases in comparison to top edge. For offshore conditions, difference between night and day is similar to that observed at top edge. For onshore, local velocities during day and night remain almost the same, except for a point at which the difference is approximately 2 m/s.

For offshore bottom edge, the change in velocity from day to night is less than 0.3m/s. For onshore bottom edge, the local velocities for day and night do not overlap and have a difference of about 1.5m/s.

CHAPTER 5

CONCLUSION AND RECOMMENDATION

Optimal harvest of wind power requires an accurate estimation of wind power potential over the area under study. To achieve this, a reliable model of atmosphere dynamics based on extensive meteorological study is paramount. Difficulty in modeling atmosphere dynamics can only be appreciated by studying the wide range of factors that influence it. A great deal of work has been done on areas such as closeness of grid, size of wind farm, effects on local climate, aerodynamics and layout of the farm. Analysis of these interdependent factors has more or less given a comprehensive idea towards design of a wind farm.

However, consistent performance of wind farms to the desired levels requires analysis of wind power potential for relatively longer periods. Current work addresses this problem by analyzing wind potential using averaged values of wind velocity for the months of January and July. WRF is a proven software which has the ability to accurately model boundary layer conditions in complex topography.

A series of six simulations were conducted over southern Oregon's coastal area using WRF. This model setup utilized three nested domains with one-way nesting and each simulation having 27 vertical hydrostatic pressure levels.

A comparative study of modeled simulations with and without wind farms was performed to obtain an overall understanding of local wind velocity. Results showed that at 10m, local wind velocity changes were quite different from that at 150m, i.e. near hub

height. Offshore and onshore simulations were conducted to analyze the effect of terrain causing such changes.

At a height of 150m, there is a reduction in wind velocity throughout the farm for all conditions. For 10m altitude, January has low turbulence and atmosphere is comparatively stable. Therefore, in vertical levels, winds are decoupled from each other as interaction is low causing differences in on-coming wind and local air temperature. This leads to increased convection causing local wind velocity to increase.

July is considered as peak summer time, turbulence is high as a result of increased convection. Therefore, there is a low temperature change inside the farm compared to its surroundings. But for onshore, presence of terrain prevents convection and hence localized increase in wind velocity.

Sources of error in WRF model can be linked to errors fed using boundary conditions provided by input files issued by NCAR. In order to increase reliability of the results obtained, more vertical levels should be added below 150m to accurately study changing vertical wind velocity due to farms. As reducing distance between wind turbines would hinder vortex breakdown, study on varying wind speed can be carried out by increasing the distance up to 15D.

REFERENCES

Adams, M.S. and David W. Keith. 2007. A Wind Farm Parameterization for WRF. Institute for Sustainable Energy, Environment, and Economy University of Calgary

Blahak, U., Bernd Goretzki and Jon Meis. 2010. A Simple Parameterization of Drag Forces Induced by Large Wind Farms for Numerical Weather Prediction Models. EWEC Conference 2010.

Carvalho, D., A. Rocha, M. Gómez-Gesteira and C. Silva Santos. 2014. Sensitivity of the WRF model wind simulation and wind energy production estimates to planetary boundary layer parameterizations for onshore and offshore areas in the Iberian Peninsula. *Applied Energy* 135: 234–246

Carvalho, D., Alfredo Rocha, Moncho Gómez-Gesteira and Carlos Santos. 2012. A sensitivity study of the WRF model in wind simulation for an area of high wind energy. *Environmental Modelling & Software* 33: 23-34

Clifford, Kevin Thomas. 2011. WRF-Model Performance for Wind Power Forecasting in the Coast Ranges of Central California. Master's Theses. Paper 4043.

Dvorak, M. J., Cristina L. Archer and Mark Z. Jacobson. 2010. California offshore wind energy potential. *Renewable Energy* 35: 1244–1254

Emami, A. and Pirooz Noghreh. 2010. New approach on optimization in placement of wind turbines within wind farm by genetic algorithms. *Renewable Energy* 35: 1559–1564

Fitch, A.C., Joseph B. Olson and Julie K. Lundquist. 2013. Parameterization of Wind Farms in Climate Models. *Journal of Climate* 26: 6439-6458, DOI: 10.1175/JCLI-D-12-00376.1.

Gao, X., Hongxing Yang and Lin Lu. 2014. Investigation into the optimal wind turbine layout patterns for a Hong Kong offshore wind farm. *Energy* 73: 430-442

Giannakopoulou, E.M. and Regis Nhili. 2014. WRF Model Methodology for Offshore Wind Energy Applications. *Advances in Meteorology.* DOI: 10.1155/2014/319819.

Gopalan, H., Christopher Gundling, Kevin Brown, Beatrice Roget, Jayanarayanan Sitaraman, Jefferey D. Mirocha and Wayne O. Miller. 2014. A coupled mesoscale–microscale framework for wind resource estimation and farm aerodynamics. *Journal of Wind Engineering and Industrial Aerodynamics* 132: 13-26.

Hanna, S. R. and R. Yang. 2001. Evaluations of Mesoscale Models' Simulations of Near-Surface Winds, Temperature Gradients, and Mixing Depths. *Journal of Applied Meteorology* 40: 1095-1104.

Janßen, H., Toni Schröder, Michael L. Zettler and Falk Pollehne. 2015. Offshore wind farms in the southwestern Baltic Sea: A model study of regional impacts on oxygen conditions. *Journal of Sea Research* 95: 248–257

Jaramillo, O. A., and M. A. Borja. 2004. Wind Speed Analysis in La Ventosa, Mexico: a Bimodal Probability Distribution Case. *Renewable Energy* 29: 1613-1630.

Kim, S.H., Hyung-Ki Shin, Young-Chul Joo and Keon-Hoon Kim. 2015. A study of the wake effects on the wind characteristics and fatigue loads for the turbines in a wind farm. *Renewable Energy* 74: 536-543.

Lu, S and Harrison M. Kim. 2014. Wind farm layout design optimization through multi-scenario decomposition with complementarity constraints. *Engineering Optimization*, DOI: 10.1080/0305215X.2013.861457

McCombs, M.P., Ryan P. Mulligan and Leon Boegman. 2014. Offshore wind farm impacts on surface waves and circulation in Eastern Lake Ontario. *Coastal Engineering* 93: 32-39.

Mehta, D., A.H. van Zuijlen, B. Koren, J.G. Holierhoek and H. Bijl. 2014. Large Eddy Simulation of wind farm aerodynamics. *Journal of Wind Engineering and Industrial Aerodynamics* 133: 1-17

Michael G. Duda, Xiang-Yu Huang, Wei Wang and Jordan G. Powers. 2008. A Description of the Advanced Research WRF Version 3. NCAR Technical Note, NCAR/TN–475+STR

Moorthy, C. B., M.K. Deshmukh and Darshana Mukherejee. 2014. New Approach for Placing Wind Turbines in a Wind Farm Using Genetic Algorithm. *Wind Engineering* 38: 633–642

Mosetti, G., Poloni C and Diviacco B. 1994. Optimization of wind turbine positioning in large wind farms by means of a genetic algorithm. *Journal of Wind Engineering and Industrial Aerodynamics* 51: 105–116.

Peña, A. and Rathmann, O. 2014. Atmospheric stability-dependent infinite wind-farm models and the wake-decay coefficient. *Wind Energy* 17: 1269–1285. doi: 10.1002/we.1632

Perveen, R., Nand Kishor and Soumya R. Mohanty. 2014. Off-shore wind farm development: Present status and challenges. *Renewable and Sustainable Energy Reviews* 29, 780–792

Roy, S.B. 2011. Simulating impacts of wind farms on local hydrometeorology. *Journal of Wind Engineering and Industrial Aerodynamics* 99: 491-498.

Salvação, N., M. Bernardino and C. Guedes Soares. 2014. Assessing mesoscale wind simulations in different environments. *Computers & Geosciences* 71: 28–36

Shaahid, S.M., Luai M. Al-Hadhrami and M. K. Rahman. 2014. Potential of Establishment of Wind Farms in Western Province of Saudi Arabia. *Energy Procedia* 52: 497 – 505.

Son, E, Seungmin Lee, Byeongho Hwang and Soogab Lee. 2014. Characteristics of turbine spacing in a wind farm using an optimal design process. *Renewable Energy* 65: 245-249.

Skamarock, W.C., Joseph B. Klemp, Jimy Dudhia, David O. Gill, Dale M. Barker, Salvação, N., M. Bernardino and C. Guedes Soares. 2015. Assessing mesoscale wind simulations in different environments. *Computers &* Geosciences 71: 28-36.

Troldberg, N. 2008. Actuator Line Modeling of Wind Turbine Wakes (Ph.D. thesis). Department of Mechanical Engineering, Technical University of Denmark, Lynby.

Volker, P., Jake Badger, Andrea Hahman and Søren Ott. 2012. Wind Farm parametrization in the mesoscale model WRF. *DTU Wind Energy*

Wang C., and Jin S. 2014. Error features and their possible causes in simulated low-level winds by WRF at a wind farm. *Wind Energy*, 17: 1315–1325 doi: 10.1002/we.1635

Wiser, R., and M. Bolinger. 2008. Annual Report on U.S. Wind Power Installation, Cost and Performance Trends: 2007. U.S. DOE Publication DOE/GO-102008-2590.

Wu, Y.T. and Fernando Porte –Agel. 2015. Modeling turbine wakes and power losses within a wind farm using LES: An application to the Horns Rev offshore wind farm. *Renewable Energy* 75: 945-955

WWEA Staff. 2010. World Wind Energy Report 2010. In 10th World Wind Energy Conference & Renewable Energy Exhibition—Greening Energy: Converting Deserts into Powerhouses (WWEC2011), Cairo, Egypt, October 31– November 2, 2011. Bonn, Germany: World Wind Energy Association.

APPENDIX A

WPS AND WRF INPUT FILES FOR JANUARY

1.1 WPS input file for January (Same for both with and without farm)

```
&share
 wrf_core = 'ARW',
 max_dom = 3,
 start_date = '2010-01-01_00:00:00','2010-01-01_00:00:00','2010-01-01_00:00:00',
 end_date   = '2010-02-01_00:00:00','2010-02-01_00:00:00','2010-01-01_00:00:00',
 interval_seconds = 21600
 io_form_geogrid = 2,
 opt_output_from_geogrid_path =
'/media/usr4/ykadiyal/oregon_final_jan/tools/WRF_domains/oregon_next/',

/

&geogrid
 parent_id         =   1,   1,  2,
 parent_grid_ratio =   1,   5,  5,
 i_parent_start    =   1,  8,   21,
 j_parent_start    =   1,  7,   9,
 e_we              =  26, 61,  91,
 e_sn              =  23,  31, 61,
 geog_data_res     = '2m','2m','2m',
 dx = 25000,
 dy = 25000,
 map_proj = 'lambert',
 ref_lat   =  43.249,
 ref_lon   = -124.539,
 truelat1  =  43.249,
 truelat2  =  43.249,
 stand_lon = -124.539,
 geog_data_path = '/media/usr4/ykadiyal/oregon_final_jan/tools/geog',
 opt_geogrid_tbl_path =
'/media/usr4/ykadiyal/oregon_final_jan/tools/WRF_domains/oregon_next/',
 ref_x = 13.0,
 ref_y = 11.5,
/

&ungrib
 out_format = 'WPS',
 prefix = 'FILE',
/

&metgrid
 fg_name = 'FILE'
 io_form_metgrid = 2,
```

/

1.2 WRF input file for January no-farm condition

```
&time_control
 run_days                            = 31,
 run_hours                           = 00,
 run_minutes                         = 0,
 run_seconds                         = 0,
 start_year                          = 2010, 2010, 2010,
 start_month                         = 01,   01,   01,
 start_day                           = 01,   01,   01,
 start_hour                          = 00,   00,   00,
 start_minute                        = 00,   00,   00,
 start_second                        = 00,   00,   00,
 end_year                            = 2010, 2010, 2010,
 end_month                           = 02,   02,   02,
 end_day                             = 01,   01,   01,
 end_hour                            = 00,   00,   00,
 end_minute                          = 00,   00,   00,
 end_second                          = 00,   00,   00,
 interval_seconds                    = 21600
 input_from_file                     = .true.,.true.,.true.,
 history_interval                    = 180,  180,   180,
 frames_per_outfile                  = 1000, 1000, 1000,
 restart                             = .false.,
 restart_interval                    = 5000,
 io_form_history                     = 2
 io_form_restart                     = 2
 io_form_input                       = 2
 io_form_boundary                    = 2
 debug_level                         = 0
 iofields_filename                   =
"my_iofields_list.txt","my_iofields_list.txt","my_iofields_list.txt",
 ignore_iofields_warning             = .true.,
 /

 &domains
 time_step                           = 150,
 time_step_fract_num                 = 0,
 time_step_fract_den                 = 1,
 max_dom                             = 3,
 e_we                                = 26,    61,   91,
 e_sn                                = 23,    31,    61,
 e_vert                              = 28,    28,    28,
 p_top_requested                     = 5000,
```

```
num_metgrid_levels            = 27,
num_metgrid_soil_levels       = 4,
dx                            = 25000, 5000,  1000,
dy                            = 25000, 5000,  1000,
grid_id                       = 1,     2,     3,
parent_id                     = 1,     1,     2,
i_parent_start                = 1,     8,    21,
j_parent_start                = 1,     7,    9,
parent_grid_ratio             = 1,     5,     5,
parent_time_step_ratio        = 1,     5,     5,
feedback                      = 1,
smooth_option                 = 0
/

&physics
mp_physics                    = 3,     3,     3,
ra_lw_physics                 = 1,     1,     1,
ra_sw_physics                 = 1,     1,     1,
radt                          = 30,    30,    30,
sf_sfclay_physics             = 1,     1,     1,
sf_surface_physics            = 2,     2,     2,
bl_pbl_physics                = 5,     5,     5,
bldt                          = 0,     0,     0,
cu_physics                    = 1,     1,     0,
cudt                          = 5,     5,     5,
isfflx                        = 1,
ifsnow                        = 0,
icloud                        = 1,
surface_input_source          = 1,
num_soil_layers               = 4,
sf_urban_physics              = 0,     0,     0,
/

&fdda
/

&dynamics
w_damping                     = 0,
diff_opt                      = 1,
km_opt                        = 4,
diff_6th_opt                  = 0,      0,      0,
diff_6th_factor               = 0.12,   0.12,   0.12,
base_temp                     = 290.
damp_opt                      = 0,
zdamp                         = 5000.,  5000.,  5000.,
```

```
dampcoef                    = 0.2,    0.2,    0.2
khdif                       = 0,      0,      0,
kvdif                       = 0,      0,      0,
non_hydrostatic             = .true., .true., .true.,
moist_adv_opt               = 1,      1,      1,
scalar_adv_opt              = 1,      1,      1,
/

&bdy_control
spec_bdy_width               = 5,
spec_zone                   = 1,
relax_zone                  = 4,
specified                   = .true., .false.,.false.,
nested                      = .false., .true., .true.,
/

&grib2
/

&namelist_quilt
nio_tasks_per_group         = 0,
nio_groups = 1,
/
```

1.3 WRF input file for January offshore condition

```
&time_control
run_days                    = 31,
run_hours                   = 0,
run_minutes                 = 0,
run_seconds                 = 0,
start_year                  = 2010, 2010, 2010,
start_month                 = 01,   01,   01,
start_day                   = 01,   01,   01,
start_hour                  = 00,   00,   0,
start_minute                = 00,   00,   00,
start_second                = 00,   00,   00,
end_year                    = 2010, 2010, 2010,
end_month                   = 02,   02,   02,
end_day                     = 01,   01,   01,
end_hour                    = 00,   00,   00,
end_minute                  = 00,   00,   00,
end_second                  = 00,   00,   00,
interval_seconds            = 21600
input_from_file             = .true.,.true.,.true.,
```

```
history_interval                    = 180,  180,   180,
frames_per_outfile                  = 1000, 1000, 1000,
restart                             = .false.,
restart_interval                    = 5000,
io_form_history                     = 2
io_form_restart                     = 2
io_form_input                       = 2
io_form_boundary                    = 2
debug_level                         = 0
iofields_filename                   =
"my_iofields_list.txt","my_iofields_list.txt","my_iofields_list.txt",
ignore_iofields_warning             = .true.,

/

&domains
time_step                           = 150,
time_step_fract_num                 = 0,
time_step_fract_den                 = 1,
max_dom                             = 3,
e_we                                = 26,    61,   91,
e_sn                                = 23,    31,    61,
e_vert                              = 28,    28,    28,
p_top_requested                     = 5000,
num_metgrid_levels                  = 27,
num_metgrid_soil_levels             = 4,
dx                                  = 25000, 5000,  1000,
dy                                  = 25000, 5000,  1000,
grid_id                             = 1,     2,     3,
parent_id                           = 1,     1,     2,
i_parent_start                      = 1,     8,    21,
j_parent_start                      = 1,     7,    9,
parent_grid_ratio                   = 1,     5,     5,
parent_time_step_ratio              = 1,     5,     5,
feedback                            = 1,
smooth_option                       = 0
/

&physics
mp_physics                          = 3,     3,     3,
ra_lw_physics                       = 1,     1,     1,
ra_sw_physics                       = 1,     1,     1,
radt                                = 30,    30,    30,
sf_sfclay_physics                   = 1,     1,     1,
sf_surface_physics                  = 2,     2,     2,
```

```
bl_pbl_physics                      = 5,     5,     5,
bldt                                = 0,     0,     0,
cu_physics                           = 1,     1,     0,
cudt                                = 5,     5,     5,
isfflx                             = 1,
ifsnow                             = 0,
icloud                              = 1,
surface_input_source               = 1,
num_soil_layers                    = 4,
sf_urban_physics                    = 0,     0,     0,
windturbines_spec                   = "ideal"
td_turbgridid                       = 3,
td_hubheight                        = 135.,
td_diameter                         = 127.,
td_stdthrcoef                       = 0.158,
td_cutinspeed                       = 3.,
td_cutoutspeed                      = 34.,
td_power                            = 7.580,
td_turbpercell                      = 1,
td_ewfx                             = 30,
td_ewfy                             = 30,
td_pwfx                             = 5,
td_pwfy                             = 15,
/

&fdda
/

&dynamics
w_damping                          = 0,
diff_opt                           = 1,
km_opt                              = 4,
diff_6th_opt                        = 0,      0,      0,
diff_6th_factor                    = 0.12,   0.12,   0.12,
base_temp                          = 290.
damp_opt                            = 0,
zdamp                               = 5000.,  5000.,  5000.,
dampcoef                            = 0.2,    0.2,    0.2
khdif                               = 0,      0,      0,
kvdif                               = 0,      0,      0,
non_hydrostatic                    = .true., .true., .true.,
moist_adv_opt                      = 1,      1,      1,
scalar_adv_opt                      = 1,      1,      1,
/
```

```
&bdy_control
spec_bdy_width                  = 5,
spec_zone                       = 1,
relax_zone                      = 4,
specified                       = .true., .false.,.false.,
nested                      = .false., .true., .true.,
/

&grib2
/

&namelist_quilt
nio_tasks_per_group      = 0,
nio_groups = 1,
/
```

1.4 WRF input file for January onshore condition

```
&time_control
run_days                    = 31,
run_hours                   = 0,
run_minutes                 = 0,
run_seconds                 = 0,
start_year                  = 2010, 2010, 2010,
start_month                 = 01,   01,   01,
start_day                   = 01,   01,   01,
start_hour                  = 00,   00,   00,
start_minute                = 00,   00,   00,
start_second                = 00,   00,   00,
end_year                    = 2010, 2010, 2010,
end_month                   = 02,   02,   02,
end_day                     = 01,   01,   01,
end_hour                    = 00,   00,   00,
end_minute                  = 00,   00,   00,
end_second                  = 00,   00,   00,
interval_seconds            = 21600
input_from_file             = .true.,.true.,.true.,
history_interval            = 180,  180,   180,
frames_per_outfile          = 1000, 1000, 1000,
restart                     = .false.,
restart_interval            = 5000,
io_form_history             = 2
io_form_restart             = 2
io_form_input               = 2
```

```
io_form_boundary                    = 2
debug_level                         = 0
iofields_filename                   =
"my_iofields_list.txt","my_iofields_list.txt","my_iofields_list.txt",
ignore_iofields_warning             = .true.,
/

&domains
time_step                           = 150,
time_step_fract_num                 = 0,
time_step_fract_den                 = 1,
max_dom                             = 3,
e_we                                = 26,    61,   91,
e_sn                                = 23,    31,    61,
e_vert                              = 28,    28,    28,
p_top_requested                     = 5000,
num_metgrid_levels                  = 27,
num_metgrid_soil_levels             = 4,
dx                                  = 25000, 5000,  1000,
dy                                  = 25000, 5000,  1000,
grid_id                             = 1,     2,     3,
parent_id                           = 1,     1,     2,
i_parent_start                      = 1,     8,    21,
j_parent_start                      = 1,     7,    9,
parent_grid_ratio                   = 1,     5,     5,
parent_time_step_ratio              = 1,     5,     5,
feedback                            = 1,
smooth_option                       = 0
/

&physics
mp_physics                          = 3,     3,     3,
ra_lw_physics                       = 1,     1,     1,
ra_sw_physics                       = 1,     1,     1,
radt                                = 30,    30,    30,
sf_sfclay_physics                   = 1,     1,     1,
sf_surface_physics                  = 2,     2,     2,
bl_pbl_physics                      = 5,     5,     5,
bldt                                = 0,     0,     0,
cu_physics                          = 1,     1,     0,
cudt                                = 5,     5,     5,
isfflx                              = 1,
ifsnow                              = 0,
icloud                              = 1,
surface_input_source                = 1,
```

```
num_soil_layers                     = 4,
sf_urban_physics                    = 0,     0,     0,
windturbines_spec                   = "ideal"
td_turbgridid                       = 3,
td_hubheight                        = 135.,
td_diameter                         = 127.,
td_stdthrcoef                       = 0.158,
td_cutinspeed                       = 3.,
td_cutoutspeed                      = 34.,
td_power                            = 7.580,
td_turbpercell                      = 1,
td_ewfx                             = 30,
td_ewfy                             = 30,
td_pwfx                             = 55,
td_pwfy                             = 15,
/

&fdda
/

&dynamics
w_damping                           = 0,
diff_opt                            = 1,
km_opt                              = 4,
diff_6th_opt                        = 0,      0,      0,
diff_6th_factor                     = 0.12,   0.12,   0.12,
base_temp                           = 290.
damp_opt                            = 0,
zdamp                               = 5000.,  5000.,  5000.,
dampcoef                            = 0.2,    0.2,    0.2
khdif                               = 0,      0,      0,
kvdif                               = 0,      0,      0,
non_hydrostatic                     = .true., .true., .true.,
moist_adv_opt                       = 1,      1,      1,
scalar_adv_opt                      = 1,      1,      1,
/

&bdy_control
spec_bdy_width                      = 5,
spec_zone                           = 1,
relax_zone                          = 4,
specified                           = .true., .false.,.false.,
nested                              = .false., .true., .true.,
/
```

```
&grib2
/

&namelist_quilt
nio_tasks_per_group      = 0,
nio_groups               = 1,
/
```

APPENDIX B

MATLAB CODE FOR MEAN VELOCITY AT 10M AND MEAN VELOCITY DIFFERENCE AT 150M

2.1 Matlab code for post processing for mean velocity difference between farm and no farm at 150m

```
clear all;
close all;
clc

n=245; %% n is time dim length
p=90;  % x-axiz length
q=60;  % y-axis length
d=7;   % 3 for night and 7 for day

%% open a netcdf file %%
ncid1 = netcdf.open('nofarm_d03-01-2.nc','NC_NOWRITE');
ncid2 = netcdf.open('offshore_d03-01.nc','NC_NOWRITE');
ncid3 = netcdf.open('onshore_d03-01.nc','NC_NOWRITE');

%% assign the variable
long = netcdf.getVar(ncid3,78,[0 0 0],[p q 1]); % longitude coordinates
lat = netcdf.getVar(ncid3,79,[0 0 0],[p q 1]); % latitude coordinates

lu = netcdf.getVar(ncid3,42,[0 0 0],[p q 1]);   % land mask index

% velocity in x and y direction on staggered grid for nofarm
u1 = netcdf.getVar(ncid1,6,[0 0 2 0],[p+1 q 1 n]);
v1 = netcdf.getVar(ncid1,7,[0 0 2 0],[p q+1 1 n]);

% velocity in x and y direction on staggered grid for offshore
u2 = netcdf.getVar(ncid2,6,[0 0 2 0],[p+1 q 1 n]);
v2 = netcdf.getVar(ncid2,7,[0 0 2 0],[p q+1 1 n]);

% velocity in x and y direction on staggered grid for onshore
u3 = netcdf.getVar(ncid3,6,[0 0 2 0],[p+1 q 1 n]);
v3 = netcdf.getVar(ncid3,7,[0 0 2 0],[p q+1 1 n]);

%%%% nofarm staggering
uf1=zeros(90,60,1,n);
vf1=zeros(90,60,1,n);
for j=1:60
for i=1:90
    uf1(i,j,:,:)=(u1(i+1,j,:,:)+u1(i,j,:,:))*0.5;
end
end

for i=1:90
    for j=1:60
            vf1(i,j,:,:)=(v1(i,j+1,:,:)+v1(i,j,:,:))*0.5;
    end
end

%%%% offshore staggering
uf2=zeros(90,60,1,n);
```

```
vf2=zeros(90,60,1,n);
for j=1:60
for i=1:90
    uf2(i,j,:,:)=(u2(i+1,j,:,:)+u2(i,j,:,:))*0.5;
end
end

for i=1:90
    for j=1:60
            vf2(i,j,:,:)=(v2(i,j+1,:,:)+v2(i,j,:,:))*0.5;
    end
end

%%%% onshore staggering
uf3=zeros(90,60,1,n);
vf3=zeros(90,60,1,n);
for j=1:60
for i=1:90
    uf3(i,j,:,:)=(u3(i+1,j,:,:)+u3(i,j,:,:))*0.5;
end
end

for i=1:90
    for j=1:60
            vf3(i,j,:,:)=(v3(i,j+1,:,:)+v3(i,j,:,:))*0.5;
    end
end

    % Mean velocity
Vm1=sqrt((uf1.^2)+(vf1.^2));
Vm2=sqrt((uf2.^2)+(vf2.^2));
Vm3=sqrt((uf3.^2)+(vf3.^2));

% Mean velocity difference between farm and no-farm
Vdiff_off=(Vm2-Vm1);
Vdiff_on=(Vm3-Vm1);


longd = double(long);
latd = double(lat);
lud=double(lu);
Vmdiff_off=double(Vdiff_off);
Vmdiff_on=double(Vdiff_on);

% plot mean difference velocity between offshore and no farm
figure(1);
sum=zeros(90,60);
a=Vmdiff_off;
b=Vmdiff_on;

for i=d:8:n  % 3 for night and 7 for day

    sum=a(:,:,i)+a(:,:,i+1)+a(:,:,i+2)+sum;
```

```
end
%mean velocity plot
avg=sum/(3*31);
h=pcolor(latd,longd,avg);
set(h,'edgecolor','none')
pca=get(gca,'position');
colorbar('westoutside')
set(gca,'position',pca)
hold all;
axes;

%Plot line dividing land and ocean
h1=contour(latd,longd,lud);
colormap hsv
axis off;

grid off
hold off

% offshore wind farm outline
rectangle('Position',[-124.93829 42.6225 0.3667 0.265], 'LineWidth',2,
'EdgeColor','black');


% plot mean difference velocity between onshore and no farm
figure(2);
sum1=zeros(90,60);
b=Vmdiff_on;
for i=d:8:n  % 3 for night and 7 for day

    sum=b(:,:,i)+b(:,:,i+1)+b(:,:,i+2)+sum1;

end

%mean velocity plot
avg1=sum1/(3*31);
h=pcolor(latd,longd,avg1);
set(h,'edgecolor','none')
pca=get(gca,'position');
colorbar('westoutside')
set(gca,'position',pca)
hold all;
axes;

%Plot line dividing land and ocean
h2=contour(latd,longd,lud);
colormap hsv
axis off;

grid off
hold off

% onshore wind farm outline
```

```
rectangle('Position',[-124.3278 42.6225 0.3667 0.265], 'LineWidth',2,
'EdgeColor','black');
```

2.2 Matlab code for post processing for local wind velocity for offshore, onshore, no farm conditions at 10 m

```
clear all;
close all;
clc

n=245; %% n is time dim length
p=90;  % x-axiz length
q=60;  % y-axis length
d=3; % 3 for night and 7 for day

%% open a netcdf file %%

ncid1 = netcdf.open('nofarm_d03-01-2.nc','NC_NOWRITE');
ncid2 = netcdf.open('onshore_d03-01.nc','NC_NOWRITE');
ncid3 = netcdf.open('offshore_d03-01.nc','NC_NOWRITE');

%Latitude and longitude cordinates
long = netcdf.getVar(ncid3,78,[0 0 0],[p q 1]);
lat = netcdf.getVar(ncid3,79,[0 0 0],[p q 1]);

%U and V at 10 m
u1 = netcdf.getVar(ncid1,31,[0 0 0],[p q n]);
v1 = netcdf.getVar(ncid1,32,[0 0 0],[p q n]);

% Land Mask Index
lu = netcdf.getVar(ncid3,42,[0 0 0],[p q 1]);

%U and V at 10 m for onshore
u2 = netcdf.getVar(ncid2,31,[0 0 0],[p q n]);
v2 = netcdf.getVar(ncid2,32,[0 0 0],[p q n]);

%U and V at 10 m for offshore
u3 = netcdf.getVar(ncid2,31,[0 0 0],[p q n]);
v3 = netcdf.getVar(ncid2,32,[0 0 0],[p q n]);

% Mean wind velocuty
Vm1=sqrt((u1.^2)+(v1.^2));
Vm2=sqrt((u2.^2)+(v2.^2));
Vm3=sqrt((u3.^2)+(v3.^2));

u1d=double(u1);
v1d=double(v1);
u2d=double(u2);
v2d=double(v2);
latd = double(lat);
longd = double(long);
Vm1d = double(Vm1);
Vm2d = double(Vm2);
Vm3d = double(Vm3);
lud = double(lu);
```

```
% to plot velocity at 10m with quiver for onshore wind farm
sum=zeros(90,60);
x=zeros(90,60);
y=zeros(90,60);
a=Vm2d;
b=u2d;
c=v2d;

for i=d:8:n  % 3 for night and 7 for day
        sum=a(:,:,i)+a(:,:,i+1)+a(:,:,i+2)+sum;
end

%mean velocity plot
avg=sum/(3*31);
h=pcolor(latd,longd,avg);
set(h,'edgecolor','none')
pca=get(gca,'position');
colorbar('westoutside')
caxis([0 14])
set(gca,'position',pca)
hold all;

%time averaging for U and V
for i=d:8:n
    x=b(:,:,i)+b(:,:,i+1)+b(:,:,i+2)+x;
    y=c(:,:,i)+c(:,:,i+1)+c(:,:,i+2)+y;
end

 %Plot every forth point in quiver
uf=zeros(90,60);
vf=zeros(90,60);
for i=1:90
    for j=1:60
        if (mod (i,4)==0)&&(mod(j,4)==0)
            uf(i,j)=x(i,j);
            vf(i,j)=y(i,j);
        end
    end
end

% plots quiver
scale_factor = 2;
h2=quiver(latd,longd,uf,vf,scale_factor);
axes;
hold all;

%Plot line dividing land and ocean
h1=contour(latd,longd,lud);
colormap hsv
axis off;

grid off
hold off
```

```
% onshore wind farm outline
rectangle('Position',[-124.3278 42.6225 0.3667 0.265], 'LineWidth',2,
'EdgeColor','black');

% to plot velocity at 10m with quiver for offshore wind farm
sum1=zeros(90,60);
x1=zeros(90,60);
y1=zeros(90,60);
a1=Vm3d;
b1=u3d;
c1=v3d;

for i=d:8:n  % 3 for night and 7 for day
  sum1=a1(:,:,i)+a1(:,:,i+1)+a1(:,:,i+2)+sum1;
end

%mean velocity plot
avg1=sum1/(3*31);
h3=pcolor(latd,longd,avg1);
set(h3,'edgecolor','none')
pca=get(gca,'position');
colorbar('westoutside')
caxis([0 14])
set(gca,'position',pca)
hold all;

%time averaging for U and V
for i=d:8:n
    x1=b1(:,:,i)+b1(:,:,i+1)+b1(:,:,i+2)+x1;
    y1=c1(:,:,i)+c1(:,:,i+1)+c1(:,:,i+2)+y1;

end

%Plot every forth point in quiver
uf1=zeros(90,60);
vf1=zeros(90,60);
for i=1:90
    for j=1:60
        if (mod (i,4)==0)&&(mod(j,4)==0)
            uf1(i,j)=x1(i,j);
            vf1(i,j)=y1(i,j);
        end
    end
end

% plots quiver
scale_factor = 2;
h4=quiver(latd,longd,uf1,vf1,scale_factor);%,'AutoScale','off');
axes;
hold all;

%Plot line dividing land and ocean
h5=contour(latd,longd,lud);
```

```
colormap hsv
axis off;
grid off
hold off

% offshore wind farm outline
rectangle('Position',[-124.93829 42.6225 0.3667 0.265], 'LineWidth',2,
'EdgeColor','black');

% to plot velocity at 10m with quiver for offshore wind farm
sum2=zeros(90,60);
x2=zeros(90,60);
y2=zeros(90,60);
a2=Vm1d;
b2=u1d;
c2=v1d;

for i=d:8:n  % 3 for night and 7 for day
  sum2=a1(:,:,i)+a1(:,:,i+1)+a1(:,:,i+2)+sum1;
end

%mean velocity plot
avg2=sum2/(3*31);
h7=pcolor(latd,longd,avg2);
set(h7,'edgecolor','none')
pca=get(gca,'position');
colorbar('westoutside')
caxis([0 14])
set(gca,'position',pca)
hold all;

%time averaging for U and V
for i=d:8:n
    x2=b2(:,:,i)+b2(:,:,i+1)+b2(:,:,i+2)+x2;
    y2=c2(:,:,i)+c2(:,:,i+1)+c2(:,:,i+2)+y2;

end

%Plot every forth point in quiver
uf2=zeros(90,60);
vf2=zeros(90,60);
for i=1:90
    for j=1:60
        if (mod (i,4)==0)&&(mod(j,4)==0)
            uf2(i,j)=x2(i,j);
            vf2(i,j)=y2(i,j);
        end
    end
end

% plots quiver
scale_factor = 2;
h8=quiver(latd,longd,uf2,vf2,scale_factor);%,'AutoScale','off');
axes;
```

```
hold all;

%Plot line dividing land and ocean
h9=contour(latd,longd,lud);
colormap hsv
axis off;
grid off
hold off
```